MASTERARBEIT | MASTER'S THESIS

Titel | Title

Establishment of in vitro assays to identify modulators of the AhR and TFEB signaling pathways

verfasst von | submitted by

Emina Pjanic BSc

angestrebter akademischer Grad | in partial fulfilment of the requirements for the degree of

Magistra pharmaciae (Mag. pharm.)

Wien | Vienna, 2026

Studienkennzahl lt. Studienblatt | Degree programme code as it appears on the student record sheet:	UA 066 605
Studienrichtung lt. Studienblatt | Degree programme as it appears on the student record sheet:	Masterstudium Pharmazie
Betreut von | Supervisor:	Assoz. Prof. Dipl.-Biochem. Dr. Elke Heiß Privatdoz.

Acknowledgment

First and foremost, my deepest gratitude goes to Assoc. Prof. Dr. Elke Heiß for providing me with the opportunity to carry out my master's thesis under her supervision. Her guidance, expertise, and continuous support were invaluable throughout this journey. The insightful feedback, encouragement, and trust she offered made this research possible and an inspiring experience.

Special thanks are due to the entire AK Dirsch team for their generous support and willingness to assist with every challenge and question that arose. I am particularly grateful for the warm and welcoming atmosphere they created, which made working with the team both highly educational and genuinely enjoyable.

I am deeply thankful to my family and friends, whose unwavering support and encouragement accompanied me throughout my studies. Their patience, understanding, and motivation provided me with strength during the most challenging moments.

Finally, special gratitude belongs to my father. Your constant belief in me, guidance, and encouragement have been my foundation throughout this journey. Completing my master's degree is a milestone I hope will make you proud.

Abstract

The increasing life expectancy of the global population has led to a growing focus on healthy aging, with the aim of maintaining physiological function and well-being at advanced age. Aging is characterized by a set of biological processes known as the hallmarks of aging, among which impaired autophagy, chronic inflammation, dysbiosis and genomic instability represent key contributing factors.

Two important cellular regulators in this context are the aryl hydrocarbon receptor (AhR) and transcription factor EB (TFEB). AhR is a ligand-activated transcription factor and a member of the xenobiotic-sensing receptor family, which regulates the expression of genes involved in xenobiotic metabolism and enhances cellular defense mechanisms against chemical and metabolic stressors. In parallel, TFEB, a member of the microphthalmia (MiT/TFE) family of transcription factors, plays a central role in the regulation of lysosomal biogenesis and autophagy by activating the transcription of autophagy–lysosomal genes.

This thesis aimed to establish two independent luciferase reporter assays for potential future screening for AhR a(nta)gonists and TFEB activators, respectively. Known ligands described in the literature were used as positive controls to validate the assays. For AhR, reporter assay results were further confirmed at the level of endogenous target genes (CYP1A1 and Ti-PARP) using quantitative real-time PCR. In addition, TFEB activation was assessed by Western blot analysis to determine changes in its phosphorylation status upon compound treatment.

The AhR reporter assay was successfully established, and well-characterized ligands were confirmed as reliable positive controls. In contrast, the TFEB assay requires further optimization to enable robust and reproducible assessment of TFEB activation.

Zusammenfassung

Die steigende Lebenserwartung der Weltbevölkerung rückt das Konzept des gesunden Alterns („healthy aging“) zunehmend in den Fokus der Forschung. Ziel ist es, nicht nur ein hohes Lebensalter zu erreichen, sondern dieses auch in möglichst guter gesundheitlicher Verfassung zu verbringen. Der Alterungsprozess kann durch die sogenannten „Hallmarks of Aging“ beschrieben werden, zu denen unter anderem eine beeinträchtigte Autophagie, chronische Entzündung, Dysbiose und Genominstabilität zählen.

Zwei zentrale Regulatoren in diesem Zusammenhang sind der Aryl-Hydrocarbon-Rezeptor (AhR) sowie der Transkriptionsfaktor EB (TFEB). Der AhR ist ein ligandaktivierter Transkriptionsfaktor und gehört zur Familie der Xenobiotika-sensitiven Rezeptoren. Er reguliert die Expression von Genen, die am Metabolismus von Fremdstoffen beteiligt sind, und trägt zur zellulären Abwehr gegenüber chemischem und metabolischem Stress bei. TFEB hingegen ist ein Mitglied der MiT/TFE-Transkriptionsfaktorfamilie und spielt eine Schlüsselrolle bei der Regulation der lysosomalen Biogenese und der Autophagie, indem er die Transkription autophagie- und lysosomenassoziierter Gene aktiviert.

Ziel dieser Arbeit war es, zwei unabhängige Luciferase-Reportergen-Assays für zukünftige Screenings nach AhR A(nta)gonisten und TFEB-Aktivatoren zu etablieren. Literaturbekannte Liganden wurden als Positivkontrollen getestet, die Assays zu validieren. Die Aktivierung des AhR wurde zusätzlich auf Ebene endogener Zielgene (CYP1A1 und TiPARP) mittels quantitativer Real-Time-PCR überprüft. Für TFEB wurde ergänzend ein Western Blot durchgeführt, um Veränderungen im Phosphorylierungsstatus des Proteins nach Behandlung mit verschiedenen Substanzen zu analysieren.

Der AhR-Reportergen-Assay konnte erfolgreich etabliert werden, und bekannte Liganden zeigten die erwartete Aktivierung, sodass sie als zuverlässige Positivkontrollen eingesetzt werden können. Im Gegensatz dazu bedarf der TFEB-Assay weiterer Optimierung, um eine robuste und reproduzierbare Analyse der TFEB-Aktivierung zu ermöglichen.

Inhaltsverzeichnis

1 Introduction

1.1 Healthy Aging

It is expected that by 2050 over 20% of the world's total population, approximately 2 billion people, will be over 60 years old. This demographic shift highlights the increasing importance of understanding the factors that influence health in older age. In this context, a growing body of evidence indicates that the aging of the immune system and a longer exposure time to risk factors play a substantial role in the multimorbidity and mortality rates of older adults. [1,2]

Aging is defined as a universal yet non-uniform physiological process, meaning that while it affects everyone, the experience of aging varies between individuals. [3] It is commonly described as a time-dependent increase in vulnerability and mortality risk. [13] At cellular level, human cells are subject to a multitude of stressors, including reactive oxygen species, non-enzymatic protein modifications, environmental substances, UV radiation, and genetic factors such as the activation of oncogenes. Together, these stressors, if not properly defeated by detoxification and repair systems, contribute to the gradual accumulation of damaged macromolecules and to a decline in cellular function that characterizes the aging process. [3]

Given the increase in life expectancy during the last decades, healthy aging has become a major goal and it is increasingly recognized in both policy and practice, including by the World Health Organization (WHO). According to the WHO, healthy aging involves the process of developing and sustaining functional abilities that allow well-being in older age. This framework highlights three central domains: intrinsic capacity, functional ability, and the environment.

Intrinsic capacity refers to the total of an individual’s physical, mental, and psychological resources, which can be further categorized into five sub-domains: locomotion, vitality, cognition, psychological aspects, and sensory functions. [4]

Functional ability, in contrast, refers to the health-related attributes that enable individuals to be and to do what they have reason to value. It is not solely determined by intrinsic capacity but results from the interaction between intrinsic capacity and the surrounding environment. [4]

The environment encompasses the broader physical, social, economic, and policy contexts in which individuals live. These environmental factors can either support or hinder the maintenance and expression of intrinsic capacity and, consequently, influence functional ability in older age. [4]

1.2 Hallmarks of Aging

Aging is a multifactorial complex which can be categorized into “hallmarks of aging” which identify cellular and molecular features that underlie biological aging processes. These hallmarks include genomic instability, telomere attrition, epigenetic alterations, loss of proteostasis, deregulated nutrient sensing, mitochondrial dysfunction, cellular senescence, stem cell exhaustion, and altered intercellular communication. [5] Beyond these originally defined hallmarks, five new hallmarks were included—compromised autophagy, microbiome disturbance, altered mechanical properties, splicing dysregulation, and chronic inflammation—as illustrated in Figure 1. Compromised autophagy has been proposed as an integrative hallmark of aging due to its involvement in multiple key processes, including proteostasis and nutrient metabolism. [5]

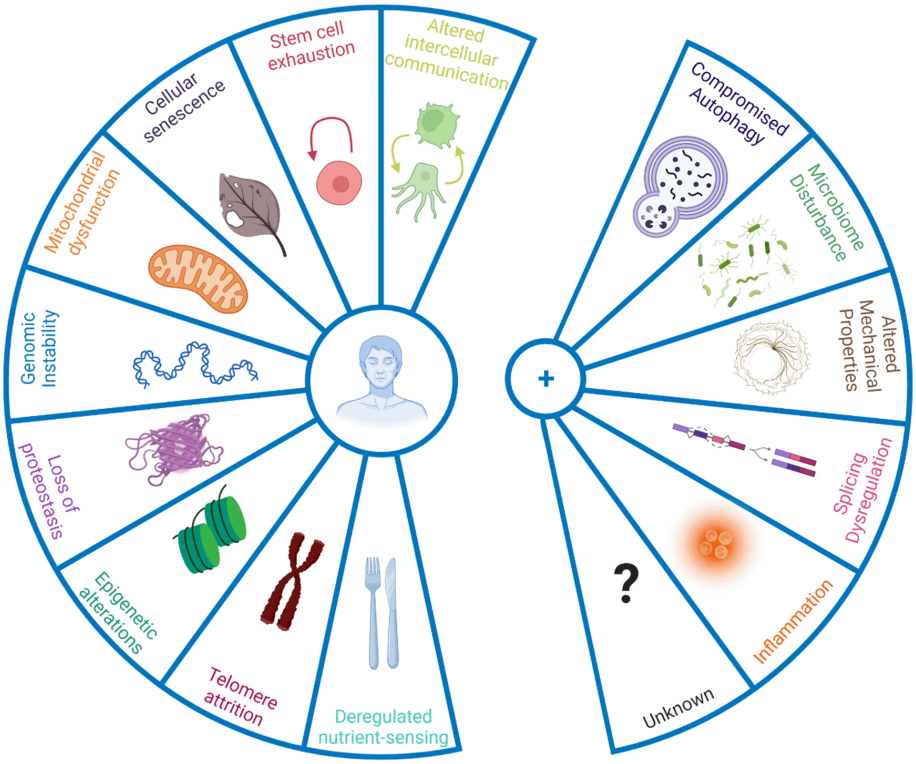

Figure 1 Hallmarks of Aging
Figure adapted from Schmauck-Medina et al.

1.2.1 Cellular stressors in Aging

Cells are constantly exposed to intrinsic and extrinsic stressors, which challenge cellular integrity and disrupt homeostasis. Cellular stress can be categorized into three major classifications: metabolic, genotoxic, and environmental, which have been demonstrated to influence significant hallmarks of aging and cellular resilience. [14,15].

Metabolic stress results from intrinsic biochemical processes, including mitochondrial activity and redox reactions. These processes generate reactive oxygen species (ROS) and lipid peroxidation products, which can modify proteins, lipids, and nucleic acids. Alongside this process, DNA damage, telomere attrition, and oncogene activation have been shown to compromise genome stability and may trigger cellular senescence, a state of irreversible cycle arrest that contributes to tissue dysfunction during the aging process. [14]. Environmental and xenobiotic stressors, including pollutants, dietary compounds, pharmaceuticals, and ultraviolet radiation also introduce reactive molecules capable of disturbing cellular metabolism and structure [16].

In order to counteract these adverse effects, avoid functional decline and foster cellular longevity, cells have developed detoxification and stress defense systems, including glutathione-dependent conjugation pathways.[16] The coordinated regulation of detoxification and repair enzymes through conserved signaling pathways maintains cellular resilience and organismal lifespan [3]. However, age-related declines in enzymatic activity may decrease the efficiency of detoxification in older individuals, which can lead to an increased susceptibility to molecular damage and contribute to the progression of aging phenotypes [17].

1.2.2 Detoxification and Xenobiotic Stress Responses

Cells have developed a detoxification system to enable them to cope with both endogenous metabolites and exogenous xenobiotics. [18,19] In order to respond to xenobiotic stress, cells run a coordinated transcriptional program that regulates enzymes responsible for biotransformation and elimination of potentially harmful compounds. [19] This program is divided into three phases. Phase I enzymes, like cytochrome P450s (CYPs), which attach reactive groups to the entered toxins. In Phase II several enzymes like glutathione S-transferases (GST), UDP-glucuronosyltransferases (UGT), catechol-O-methyltransferases (COMT), and N-acetyltransferases (NAT), add water-soluble groups onto the molecule. Phase III is known for facilitating the export of the modified conjugate out of the cell through ATP-binding cassettes (ABC) transporter proteins. [20]

Among the transcriptional regulators of xenobiotic metabolism, the aryl hydrocarbon receptor (AhR) plays a central role. Activation of AhR induces the expression of multiple detoxification enzymes and enhances cellular defense capacity against environmental and metabolic stressors [21,22]. Beyond its classical detoxification function in mammals, AhR signaling has been also linked to stress-resistance pathways and longevity regulation in several model organisms, including *Caenorhabditis elegans* [23,24].

1.2.3 Aryl Hydrocarbon Receptor

The aryl hydrocarbon receptor (AhR) is a ligand-activated transcription factor and a member of the xenobiotic-sensing receptor (XR) family. It belongs to the basic helix–loop–helix Per–ARNT–Sim (bHLH–PAS) protein family and is broadly distributed across human tissues, particularly in organs involved in detoxification and barrier function such as the lung, liver, kidney, and placenta [23–25]. In its inactive state, AhR resides in the cytosol and responds to both endogenous and exogenous ligands, including environmental xenobiotics and metabolic intermediates. Upon activation, AhR regulates the transcription of genes involved in xenobiotic metabolism and enhances cellular defense capacity against chemical and metabolic stressors [21–23].

Beyond its classical role in detoxification, AhR has a multifunctional regulator function, influencing cellular processes such as proliferation, immune modulation, and stress adaptation. [23,24]

1.2.3.1 AhR signalling pathway

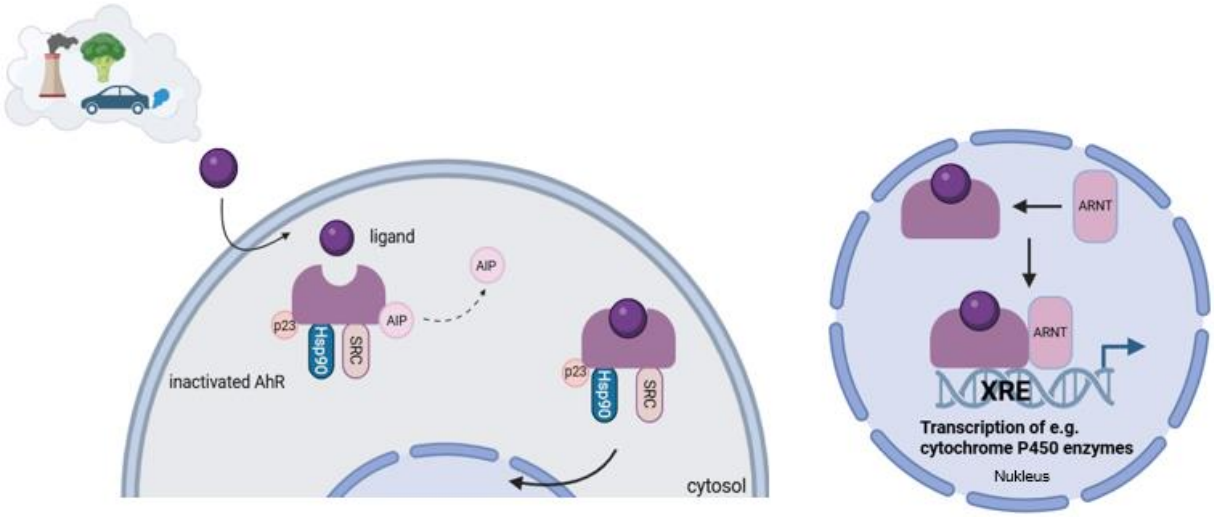

Figure 2 The canonical Aryl Hydrocarbon Receptor pathway, created on Biorender.com

AhR = Aryl Hydrocarbon Rezeptor

During the inactive phase the receptor resides in the cytoplasm as part of a multiprotein chaperone complex. This complex contains a dimer of the 90-kDa heat shock protein (HSP90), the AHR-interacting protein (AIP or XAP2/ARA9), the co-chaperone p23, and the

tyrosine kinase SRC [25, 26, 28]. HSP90 has been shown to stabilize both the PAS and bHLH domains of AhR, while AIP has been demonstrated to promote cytoplasmic retention by inhibiting interaction with importin-β. The co-chaperone p23 plays a critical role in protecting AhR from ubiquitin-mediated degradation [28]. The receptor is maintained in a conformation with high affinity for ligand binding [28].

Upon ligand binding, a conformational change occurs, resulting in partial dissociation of AIP and other chaperones, and exposure of the N-terminal nuclear localization signal (NLS) [26-28]. The ligand-AhR complex translocates then into the nucleus through an importin-β-dependent mechanism, a process that can be modulated by phosphorylation events [28]. After entering the nucleus, AhR heterodimerizes with the AHR nuclear translocator (ARNT) and binds to xenobiotic response elements (XREs; consensus sequence 5'-TNGCGTG-3') located in the promoter regions of target genes. [25,27,28]

This interaction is known to induce the transcription of AhR target genes, including CYP1A1, CYP1A2, and CYP1B1, which are involved in the metabolism of xenobiotics and endogenous substrates. [25,27] Furthermore, the recruitment of co-activators has been demonstrated to enhance chromatin accessibility and facilitate transcriptional activation. [26]

The process of AhR signaling is regulated by a series of negative feedback mechanisms, which serve to balance and regulate its activity. Among the directly induced target genes are the AhR repressor (AHRR) and the TCDD-inducible poly(ADP-ribose) polymerase (TIPARP/TiPARP). [25-27] AHRR demonstrates competition with ligand-activated AHR for ARNT binding and XRE occupancy, thereby inhibiting AHR-driven transcription. [26-28] TIPARP's mechanism of action involves the attenuation of signaling through the ADP-ribosylation of AhR, leading to its subsequent proteasomal degradation. [26,27] Additionally, the activation of AhR by a ligand results in ubiquitination, which inactivates the receptor and promotes its degradation by the 26S proteasome. [26, 27]

The induction of CYP1 enzymes has also been demonstrated to contribute to a functional negative feedback loop by metabolizing and thereby eliminating AhR ligands. [26]

Altogether, AhR signal transduction is a highly regulated process characterized by precisely coordinated activation, attenuation and termination mechanisms. Such tight

control likely prevents excessive or chronic pathway activation and underscores the role of AhR as a central mediator of cellular homeostasis and adaptation to environmental and metabolic stressors. [26,28]

1.2.3.2 Ligands and activators of AhR

1.2.3.2.1 Selected Exogenous Ligands

Among the exogenous AHR ligands is benzo[a]pyrene (BaP), a polycyclic aromatic hydrocarbon generated during incomplete combustion of organic material (Figure 3). BaP binding to AHR induces transcription of CYP1A1 and CYP1B1, leading to metabolic activation and formation of reactive intermediates (26, 30). While this represents a classical detoxification response, prolonged or excessive activation may increase oxidative burden and DNA damage, processes associated with cellular aging. [28, 29]

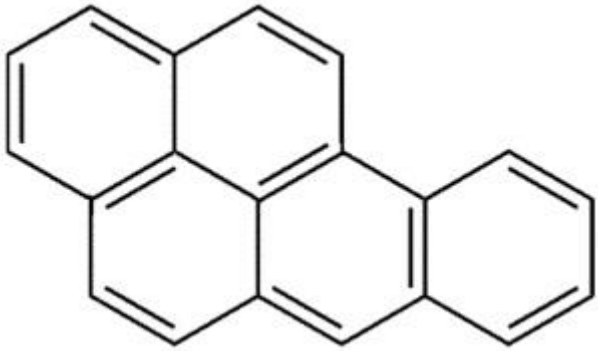

Figure 3 Benzo[a]pyrene (exogenous environmental ligand

In addition to environmental pollutants, dietary-derived compounds can modulate AhR activity. Indole-3-carbinol (I3C) (Figure 4), found in cruciferous vegetables e.g. broccoli, undergoes acid-catalyzed condensation in the stomach to generate AhR-active metabolites. [22,30] Compared to persistent toxic ligands, dietary indoles are generally rapidly metabolized and may support balanced AhR activation and redox homeostasis. [43]. The parent I3C has also been observed to bind to and activate the AhR directly, however, with relatively low affinity. [44]

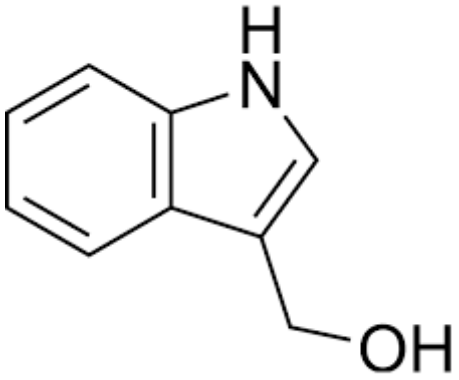

Figure 4 Indole-3-carbinol (dietary precursor)

Synthetic AhR agonists such as I3MO (3-indolylmethanamine derivatives, indirubin 3-monoxime) (Figure 5) have been developed to selectively modulate AHR signaling and are being explored for anti-inflammatory applications [27]. These compounds highlight the therapeutic potential of controlled AhR activation in aging-associated inflammatory and metabolic conditions.

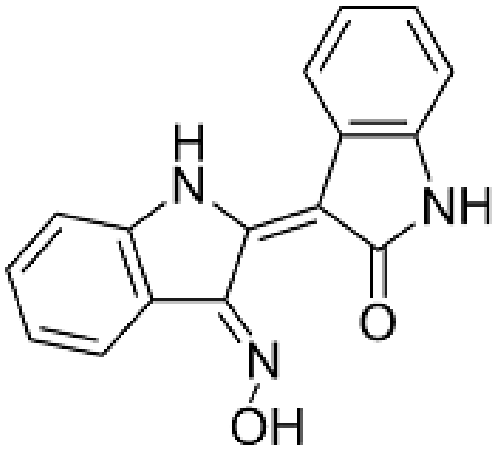

Figure 5 I3MO (synthetic agonist)

1.2.3.2.2 A selected endogenous Ligand

AhR responds to endogenous metabolites too. One of the most potent ligands is 6-formylindolo[3,2-b]carbazole (FICZ) (Figure 6), a tryptophan-derived photoproduct generated upon UV exposure [31,32]

FICZ induces strong AhR activation followed by efficient metabolic clearance through CYP1 enzymes, establishing a tightly controlled negative feedback loop [26,33] Importantly, aging is characterized by altered xenobiotic metabolism, increased oxidative stress, and changes in tryptophan metabolism. [22,26]

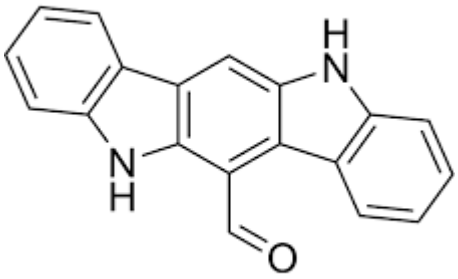

Abbildung 6 6-Formylindolo[3,2-b]carbazole (endogenous ligand)

1.2.4 Autophagy in Aging and Cellular Homeostasis

Autophagy identifies and removes old or damaged cell components by enclosing them in autophagosomes for disposal or recycling, making room for new structures and conserving resources. It also supplies metabolites—amino acids, lipids, carbohydrates, and nucleic acids—particularly during stress or nutrient shortages. [7, 8, 9] A age-dependent decline in autophagy has been associated with neurodegenerative diseases such as Alzheimer's, Parkinson's or Huntington's disease. [7], and a boost in of autophagy has been found to be positively correlated with a longer healthy lifespan [46]

1.2.5 Transcription Factor EB

The transcription factor EB (TFEB), a member of microphthalmia (MiT/TFE) family of leucine zipper transcription factors, is a key regulator of the expression of genes involved in lysosome biogenesis and autophagy. TFEB can form homo- or heterodimers with itself or other members of the MiT/TFE family, binding to CLEAR (Coordinated Lysosomal Expression and Regulation) elements to activate the transcription of autophagy-lysosomal genes, which results then in a higher amount of lysosomes.[9,10]

Beyond its role in autophagy and lysosome biogenesis, TFEB also participates in metabolic regulation and the maintenance of cellular energy homeostasis in response to both internal and external stress signals.[10]

Therefore, TFEB agonists, i.e. compounds with an activating influence on TFEB activity, have emerged as potential therapeutic agents for diseases characterized by autophagy-lysosomal dysfunction. The regulatory network governing TFEB activity is highly complex, and research on compounds that activate TFEB is rapidly expanding. Notably, certain TFEB agonists, such as rapamycin, have already been approved for clinical use in oncology[11] and have also been reported as promising compounds for increasing lifespan across species . [47]

1.2.5.1 TFEB signalling pathway

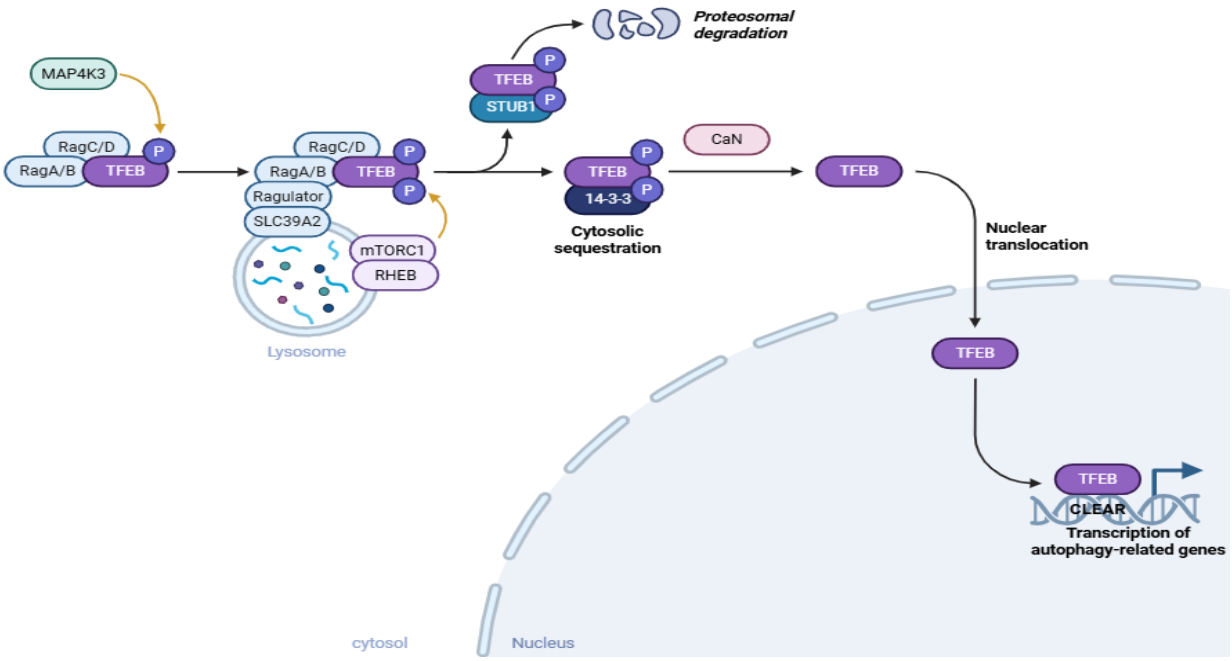

Figure 7 TFEB pathway, adapted from Biorender.com

Under nutrient-rich conditions, amino acids activate the Rag GTPases (RagA or RagB in complex with RagC or RagD), which recruit mechanistic target of rapamycin complex 1 (mTORC1) to the lysosomal surface. The Rag GTPases are fixed to the lysosomal membrane by the Ragulator complex. MAP4K3 has been identified as an upstream kinase that reacts to amino acid availability and contributes to mTORC1 activation, thereby creating a connection between nutrient status and downstream signaling events [34,35].

Once localized to the lysosomal membrane, mTORC1 becomes fully activated through interaction with Rheb-GTP. Active mTORC1 directly phosphorylates TFEB at specific serine residues, namely Ser122, Ser142, and Ser211, thereby regulating its cytoplasmic retention and transcriptional activity. [45] Phosphorylated TFEB interacts with 14-3-3 adaptor proteins, which retain it in the cytoplasm by masking its nuclear localization signal. In this phosphorylated state, TFEB is transcriptionally inactive, and expression of lysosomal and autophagy-related genes is suppressed [34-36].

Upon low nutrient conditions Rag GTPases changes to their inactive nucleotide-bound state, leading to dissociation of mTORC1 from the lysosomal surface. The activity of mTORC1 is reduced due to decreased signaling through the Rheb pathway. As mTORC1 activity declines, TFEB is no longer efficiently phosphorylated. Dephosphorylation of TFEB leads to reduced interaction with 14-3-3 proteins and exposes its nuclear localization sequence, enabling translocation into the nucleus. Calcium-dependent phosphatases, such as calcineurin, have also been implicated in promoting TFEB dephosphorylation under stress conditions [35-37].

After nuclear translocation, TFEB binds to coordinate lysosomal expression and regulation (CLEAR) elements in the promoters of its target genes. This induces a transcriptional program that forces lysosomal biogenesis, autophagosome formation and lysosomal enzyme production. TFEB regulates genes involved in lipid catabolism and metabolic adaptation, thereby coordinating cellular clearance mechanisms with energy homeostasis [35-38].

The functional outcome of TFEB activation is an expansion of the lysosomal compartment and increased autophagic flux, promoting degradation of damaged proteins, dysfunctional mitochondria, and aggregated macromolecules. Through this nutrient-responsive lysosomal signaling axis—MAP4K3, Rag GTPases, Ragulator, mTORC1, and TFEB—the cell dynamically adjusts its degradative capacity to metabolic and environmental conditions. This ability to balance proteostasis and cellular homeostasis is essential for maintaining internal equilibrium. [34-38].

1.2.5.2 Activators of TFEB

Pharmacological activation of TFEB has been intensively researched to investigate its regulatory mechanisms and to enhance lysosomal–autophagic function.
Rapamycin, a macrolide acts as an allosteric inhibitor of mTORC1, leading to reduced mTORC1-dependent phosphorylation of TFEB. This reduction promotes TFEB nuclear translocation and results in increased transcription of CLEAR network genes [39,40]
Since rapamycin incompletely inhibits specific mTORC1 substrates, ATP-competitive inhibitors such as Torin1 (Figure 8) induce a more comprehensive inhibition of mTOR

kinase activity. Consequently, this results in more pronounced TFEB dephosphorylation and enhanced nuclear accumulation relative to rapamycin (Figure 9) [40]

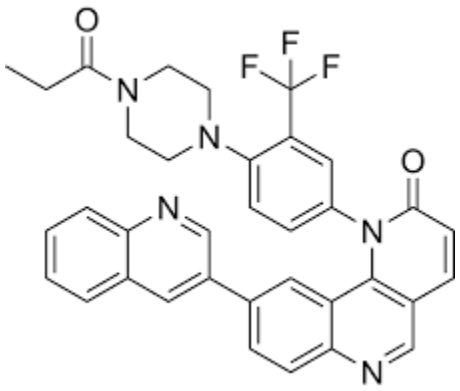

Figure 8 Torin1

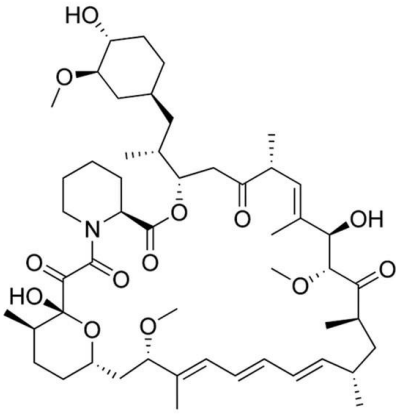

Figure 9 Rapamycin

An alternative approach to activate TFEB involves the curcumin-derived compound C1 (Figure 10). Unlike mTOR inhibitors, C1 stimulates TFEB independently of mTORC1 signaling. It directly interacts with TFEB and promotes its translocation from the cytoplasm to the nucleus without requiring upstream inhibition of mTOR activity. As a result, TFEB can initiate its transcriptional program under conditions where mTOR signaling remains unchanged. Once in the nucleus, TFEB binds to CLEAR (Coordinated Lysosomal Expression and Regulation) elements in the promoter regions of autophagy- and lysosome-related genes, thereby enhancing lysosomal biogenesis and autophagic activity. [42]

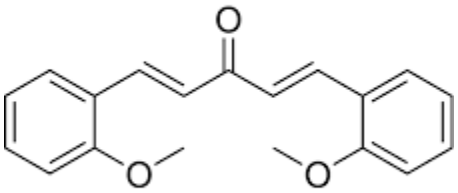

Figure 10 TFEB-activator C1

In addition, TFEB can also be activated via calcium-mediated pathways. Thapsigargin (Figure 11), a SERCA inhibitor, increases cytosolic Ca^{2+} levels and activates calcineurin, which directly dephosphorylates TFEB and promotes its nuclear translocation independently of nutrient availability [41].

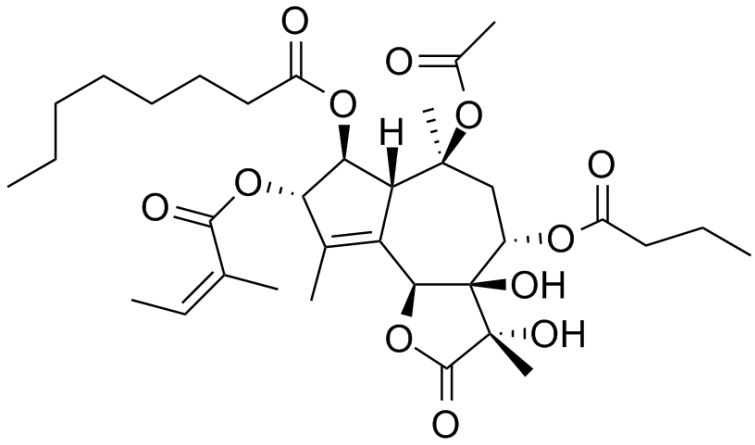

Figure 11 Thapsigargin (SERCA-Inhibitor)

Overall, TFEB activation can be achieved through both mTOR-dependent and calcium-dependent mechanisms as well as direct binding - highlighting TFEB as a central integrator of nutrient and stress signalling pathways controlling lysosomal biogenesis and autophagy.

2 Research objective and research approach

The aim of this thesis was to set up in vitro reporter gene assays in the lab to identify modulators of the cellular defense pathways controlled by AhR and TFEB. For this purpose, Caco-2 and HepG2 cells were transfected with plasmid constructs containing XRE or 2X/4X CLEAR-driven luciferase reporter genes. As a control for transfection efficiency, cells were co-transfected with an EGFP expression plasmid.

Following transfection, the cells were treated with various known ligands and activators, of the given target and pathway activation was assessed using a luciferase reporter assay. In parallel, qPCR analyses were performed to confirm the induction of endogenous target genes, such as *CYP1A1* and *TiPARP* for AhR, while Western blot experiments were conducted to determine the TFEB phosphorylation status.

Finally, a small-scale screening was performed, including selected gut metabolites of polyphenols and a set of previously uncharacterized phyllobillins (kindly provided by Prof. Simone Moser, University of Innsbruck), to identify potential modulators of these pathways.

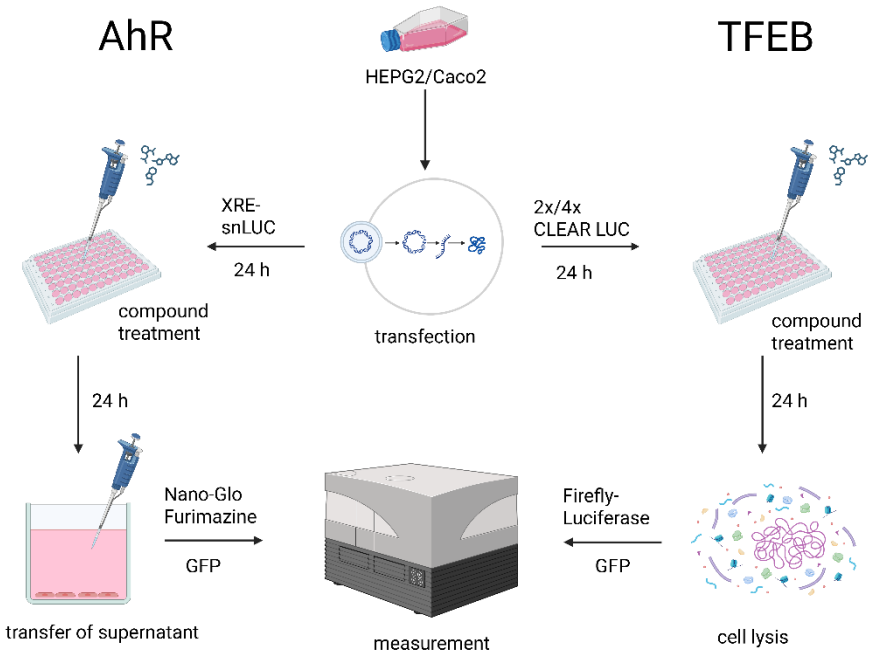

Figure 12 Workflow for luciferase assays, created on Biorender.com

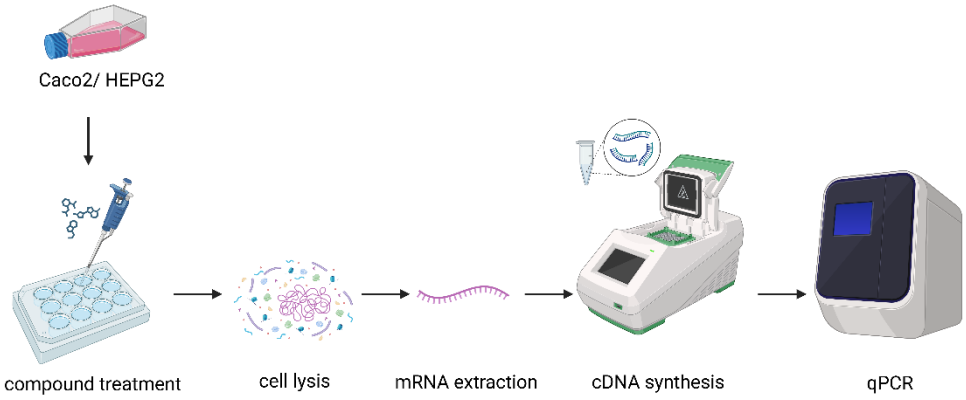

Figure 13 Workflow for qPCR analyses, created on Biorender.com

3 Results and Discussion

3.1 Establishment of the assays

3.1.1 Optimization of transfection parameters

Prior to functional analysis, transfection parameters for HepG2 and Caco2 Cells needed to be optimized. Transfection efficiency was evaluated using an EGFP expression plasmid as a marker for both flow cytometry and fluorescence microscopy, with flow cytometry providing quantitative assessment of transfection efficiency and microscopy confirming cellular expression patterns. These analyses demonstrated that transfection efficiency was strongly influenced by DNA amount, cell density, and P3000 concentration. Initial experiments showed that lower DNA amounts (250 ng per well at 300,000 cells in a 6 well plate) resulted in the highest proportion of EGFP-positive cells, whereas higher DNA amounts (500 ng) further increased fluorescence intensity per cell (Figure 14). Optimization of P3000 concentrations indicated that higher reagent amounts improved transfection efficiency at higher cell densities.

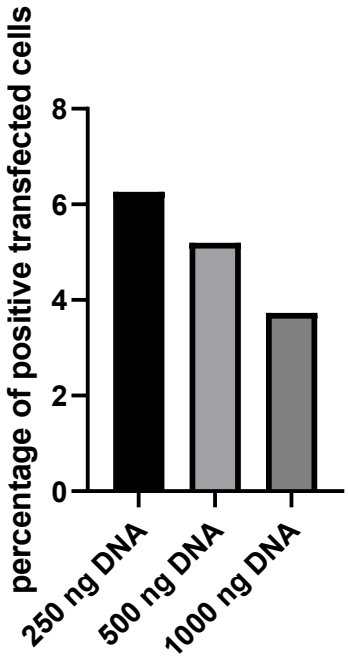

Figure 14 HepG2 cells (300,000 cells per well, 6-well plate) were transfected with an EGFP expression plasmid under varying conditions. Transfection efficiency was determined by flow cytometry as the percentage of EGFP-positive cells and confirmed by fluorescence microscopy. DNA amounts of 250 ng and 500 ng per well were tested. Data represent a single experiment (n = 1).

3.1.2 XRE- and CLEAR-driven reporter gene assays

To investigate AhR-dependent transcription, a XRE-driven luciferase reporter assay was employed using the XRE-pNL1.3[secNLuc] construct in HepG2 and Caco2 cells. As mentioned above, transfection conditions were adjusted to achieve efficient expression, with 30,000 cells per well in a 96-well format and 100 ng total plasmid per well (75 ng reporter plasmid and 25 ng EGFP for monitoring transfection efficiency) using Lipofectamine 3000 with 0.2 µL P3000 reagent. Compound treatment was initiated 24 h post-transfection in fresh medium, and luciferase activity was measured at 5 h and 24 h post-treatment. The 5 h measurement often exceeded the detection limit of the plate reader, indicating a strong boost of reporter activation but preventing accurate quantification. Therefore, a 24 h treatment duration was used for all subsequent experiments to ensure signals easily fell within the dynamic range of the detection system.

Luciferase activity was measured using the Promega Nano-Glo® Luciferase assay kit. To account for differences in transfection efficiency and cell number, luminescence values were background-corrected using untransfected control wells and then normalized to fluorescence from co-transfected EGFP. Fold induction was calculated relative to DMSO-treated controls, which were set to 1.0.

This optimization ensured that the assay produced robust and reproducible signals, allowing accurate assessment of AhR-dependent transcriptional responses.

A standard “home-made” luciferase assay was used for the CLEAR-driven firefly reporter luciferase. Signals were also background-corrected and normalized to EGFP fluorescence to account for differences in transfection efficiency and cell number, and values were expressed as fold change relative to DMSO-treated controls.

Comparison of CLEAR constructs containing two or four CLEAR elements showed that the 4x CLEAR construct consistently produced higher luciferase signals, reflecting an increased dynamic range and improved sensitivity. These initial optimizations were basis for further detection of treatment-induced transcriptional changes in the targeted reporter gene assays.

3.2 Activation of XRE reporter gene expression in HepG2 and Caco-2 cells by the selected known AhR- agonists

3.2.1 XRE-driven luciferase expression in HepG2 and Caco-2 cells upon exposure to FICZ

Treatment with FICZ resulted in a concentration-dependent induction of XRE-driven luciferase activity in both HepG2 and Caco-2 cells (Figures 15 and 16). In HepG2 cells (Figure 14), stimulation with 10 nM FICZ increased XRE activity to approximately 13-fold compared to the DMSO control, whereas 100 nM FICZ led to a stronger approx. 30-fold induction. In Caco-2 cells (Figure 15), FICZ elicited a markedly higher response. Treatment with 10 nM resulted in an approximately 80-fold induction, while 100 nM FICZ increased XRE activity to approximately 130–140-fold relative to DMSO-treated controls.

Overall, FICZ induced AhR activation and XRE-driven reporter gene expression in both cell lines, with a stronger response observed in Caco-2 cells.

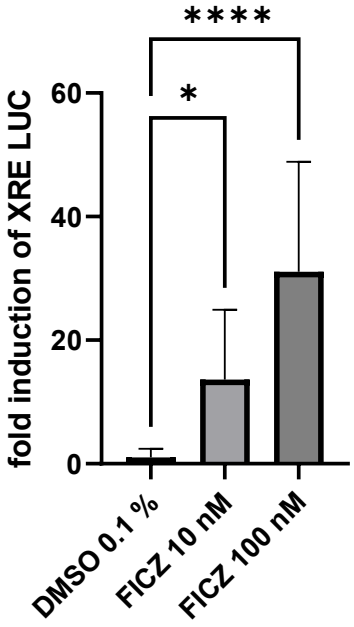

Figure 15 FICZ induces XRE-driven luciferase activity in HepG2 cells. Transfected HepG2 cells were treated with 10 nM or 100 nM FICZ or 0.1% DMSO as vehicle control for 24 h. Luciferase activity was measured using a secreted luciferase reporter system. Raw luminescence and fluorescence values were corrected by subtracting signals from untransfected cells. Luciferase activity was normalized to fluorescence (Lum/Flu) and expressed as fold change relative to the mean of DMSO-treated controls. Data represent n = 3 independent experiments. Statistical significance was determined using one-way ANOVA followed by multiple comparisons test. $p < 0.0001$ vs DMSO. Not significant is not shown.

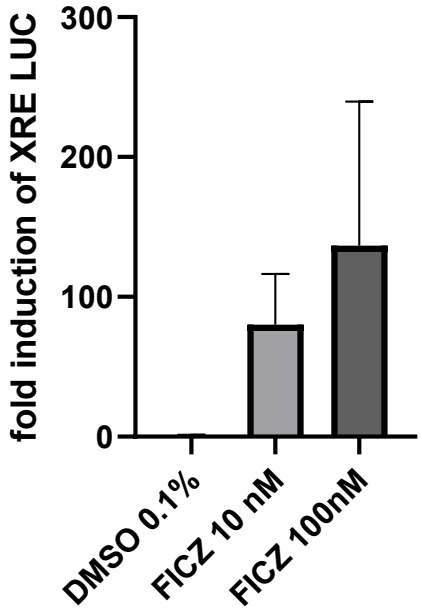

Figure 16 FICZ induces XRE-driven luciferase activity in Caco-2 cells. Transfected Caco-2 cells were treated with 10 nM or 100 nM FICZ or 0.1% DMSO as vehicle control for 24 h. Luciferase activity was measured using a secreted luciferase reporter system. Raw luminescence and fluorescence values were corrected by subtracting signals from untransfected cells. Luciferase activity was normalized to fluorescence (Lum/Flu) and expressed as fold change relative to the mean of DMSO-treated controls. Data represent n = 1-2 independent experiments.

3.2.2 XRE-driven luciferase expression in HepG2 and Caco-2 cells upon exposure to BaP

Treatment with BaP resulted in a concentration-dependent activation of the XRE-driven luciferase reporter in both HepG2 and Caco-2 cells (Figures 17 and 18). However, the magnitude of induction differed between the two cell lines.

In HepG2 cells, BaP induced a gradual increase in reporter activity across the tested concentration range (Figure 17). While 0.3 µM BaP led to an approximately 3-fold induction relative to DMSO-treated controls, 1 µM increased the response to around 4-fold, and 3 µM resulted in an induction of approximately 6-fold.

In Caco-2 cells, BaP reached a stronger response (Figure 18). Already at 0.3 µM, XRE activity was elevated to approximately 18-fold compared to DMSO-treated controls. Increasing concentrations further enhanced reporter activity, reaching approximately 23-fold at 1 µM and around 30-fold at 3 µM.

Overall, BaP activated AhR-dependent transcription in both cell lines, with a substantially stronger induction observed in Caco-2 cells compared to HepG2 cells under the same experimental conditions, as already seen for FICZ.

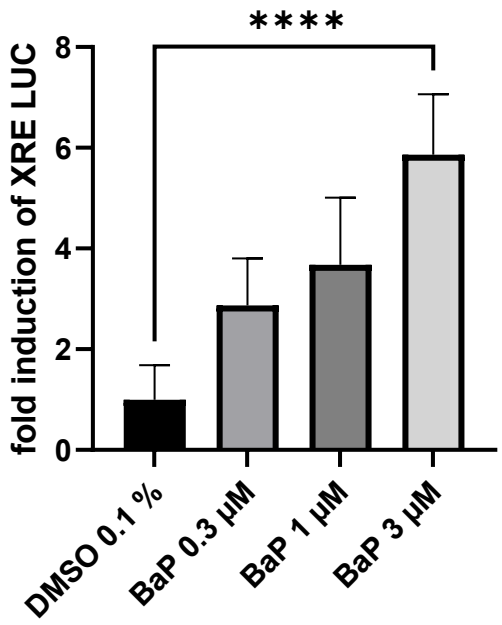

Figure 17 Benzo[a]pyrene (BaP) induces XRE-driven luciferase activity in HepG2 cells. Transfected HepG2 cells were treated with 0.3 µM, 1 µM, or 3 µM BaP or 0.1% DMSO as vehicle control for 24 h. Luciferase activity was measured using a secreted luciferase reporter system. Raw luminescence and fluorescence values were corrected by subtracting signals from untransfected cells. Luciferase activity was normalized to fluorescence (Lum/Flu) and expressed as fold change relative to the mean of DMSO-treated controls. Data represent n = 1–4 independent experiments.
Statistical significance was determined using one-way ANOVA followed by multiple comparisons test. p < 0.0001 vs DMSO. Not significant is not shown.

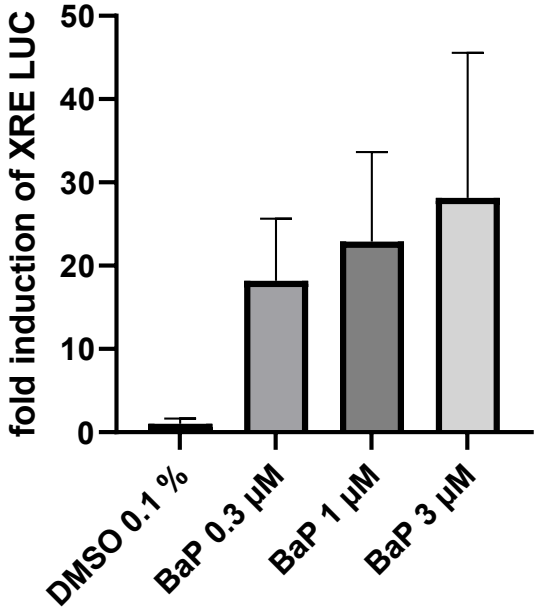

Figure 18 Benzo[a]pyrene (BaP) induces XRE-driven luciferase activity in Caco-2 cells. Transfected Caco-2 cells were treated with 0.3 µM, 1 µM, or 3 µM BaP or 0.1% DMSO as vehicle control for 24 h. Luciferase activity was measured using a secreted luciferase reporter system. Raw luminescence and fluorescence values were corrected by subtracting signals from untransfected cells. Luciferase activity was normalized to fluorescence (Lum/Flu) and expressed as fold change relative to the mean of DMSO-treated controls. Data represent n = 2 independent experiments.

3.2.3 XRE-driven luciferase expression in HepG2 and Caco-2 cells upon exposure to I3C

Treatment with I3C resulted in a cell line–specific activation pattern of the XRE-driven luciferase reporter, with differences in the extent of concentration dependency.

In HepG2 cells, I3C induced only a moderate increase in reporter activity across the tested concentration range (Figure 19). While lower concentrations (0.3–3 µM) resulted in only slight increases compared to DMSO-treated controls, 10 µM I3C led to an induction of approximately 2-fold. Overall, the increase in XRE activity remained low, in line with the low affinity of the unmetabolized I3C to AhR.

In Caco-2 cells, a distinct response pattern was observed (Figure 20). At lower concentrations (0.3–3 µM), I3C had minimal effects on luciferase activity, with values comparable to the DMSO control. However, at 10 µM, a pronounced increase in XRE-driven reporter activity was detected, reaching approximately 18–20-fold induction.

To assess whether the strong induction observed at the highest concentration was associated with cytotoxic effects, GFP fluorescence values were analyzed. As GFP levels were comparable to those of the DMSO control, no indication of cytotoxicity was observed under these conditions.Taken together, I3C induced only weak AhR-dependent transcription in HepG2 cells, compared to Caco-2 cells. This is consistent with previous reports indicating that transient AhR/XRE reporter activity in HepG2 is generally low, while Caco-2 cells show stronger responses, likely due to higher receptor expression, greater co-factor availability, and a more permissive cellular context for xenobiotic signaling [53,54]. These cell type-specific differences explain why the tested compounds produced lower luciferase activity in HepG2 than in Caco-2 under identical experimental conditions.

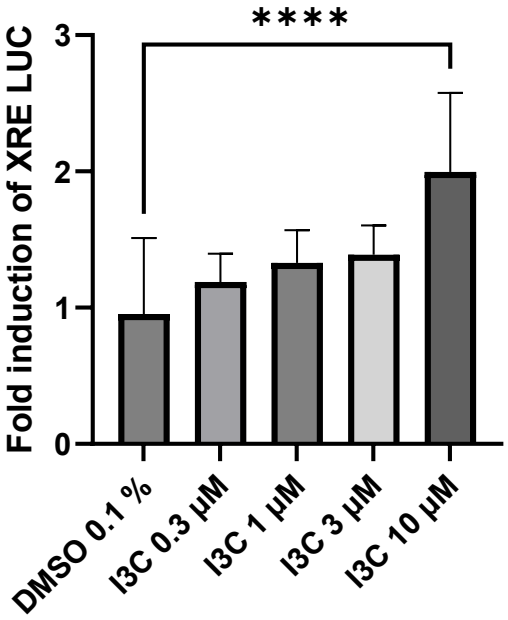

Figure 19 I3C induces XRE-driven luciferase activity in HepG2 cells. Transfected HepG2 cells were treated with 0.3 µM, 1 µM, 3 µM, or 10 µM I3C or 0.1% DMSO as vehicle control for 24 h. Luciferase activity was measured using a secreted luciferase reporter system. Raw luminescence and fluorescence values were corrected by subtracting signals from untransfected cells. Luciferase activity was normalized to fluorescence (Lum/Flu) and expressed as fold change relative to the mean of DMSO-treated controls. Data represent n = 1–4 independent experiments.
Statistical significance was determined using one-way ANOVA followed by multiple comparisons test. $p < 0.0001$ vs DMSO. Not significant is not shown.

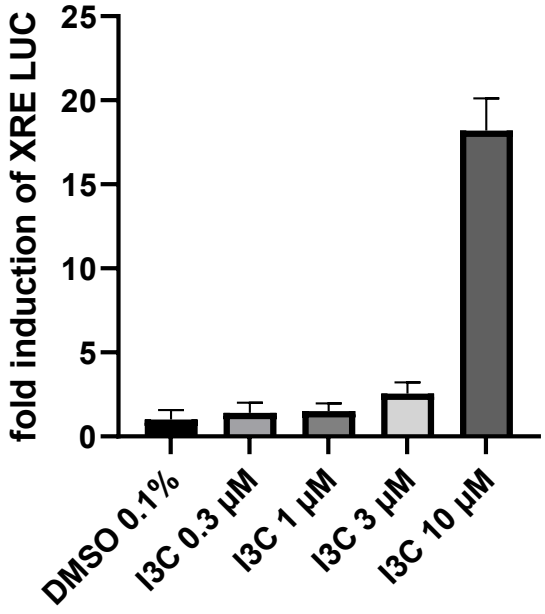

Figure 20 3C induces XRE-driven luciferase activity in Caco-2 cells. Transfected Caco-2 cells were treated with 0.3 µM, 1 µM, 3 µM, or 10 µM I3C or 0.1% DMSO as vehicle control for 24 h. Luciferase activity was measured using a secreted luciferase reporter system. Raw luminescence and fluorescence values were corrected by subtracting signals from untransfected cells. Luciferase activity was normalized to fluorescence (Lum/Flu) and expressed as fold change relative to the mean of DMSO-treated controls. Data represent n = 2 independent experiments.

3.2.4 XRE-driven luciferase expression in HepG2 and Caco-2 cells upon exposure to I3MO

Treatment with Indirubin-3'-monoxime (I3MO) resulted in a concentration-dependent activation of the XRE-driven luciferase reporter in both cell lines.

In HepG2 cells, I3MO induced reporter activity 7-16 fold across the tested concentration range (Figure 21). Compared to the DMSO control (0.1%), which showed minimal basal activity, treatment with 0.1 µM I3MO led to a noticeable 7-fold increase in XRE-driven luciferase expression. Increasing concentrations (0.3–3 µM) further enhanced reporter activity, with the highest 16-fold induction observed at 3 µM.

In Caco-2 cells, a similar but again more pronounced activation pattern was observed (Figure 22). While the DMSO control again exhibited only minimal reporter activity, treatment with 0.1 µM I3MO resulted in a more than 30-fold increase in XRE-driven luciferase expression. Comparable induction levels were observed at 0.3 µM, whereas the highest concentration (3 µM) led to the strongest activation of the XRE reporter with around 50x induction. The overall fold induction in Caco-2 cells was markedly higher than that observed in HepG2 cells.

Taken together, these results demonstrate that I3MO induces XRE-mediated transcription in a concentration-dependent manner in both cell lines, with a stronger activation observed in Caco-2 cells compared to HepG2 cells.

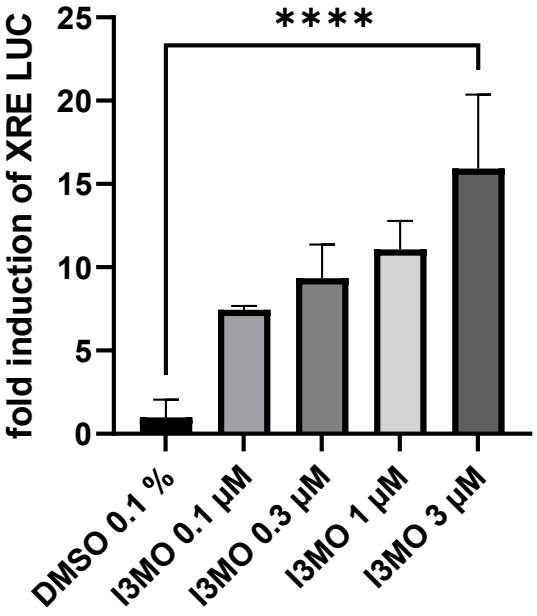

Figure 21 I3MO induces XRE-driven luciferase activity in HepG2 cells. Transfected HepG2 cells were treated with 0.1 µM, 1 µM, or 3 µM I3MO or 0.1% DMSO as vehicle control for 24 h. Luciferase activity was measured using a secreted luciferase reporter system. Raw luminescence and fluorescence values were corrected by subtracting signals from untransfected cells. Luciferase activity was normalized to fluorescence (Lum/Flu) and expressed as fold change relative to the mean of DMSO-treated controls. Data represent n = 1–4 independent experiments.
Statistical significance was determined using one-way ANOVA followed by multiple comparisons test. $p < 0.0001$ vs DMSO. Not significant is not shown.

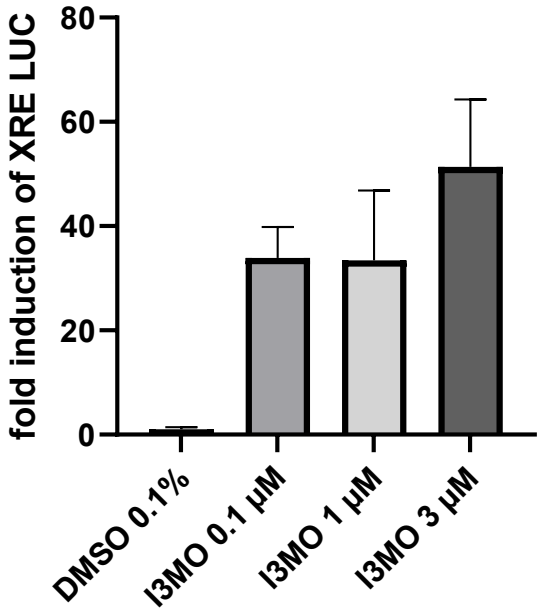

Figure 22 I3MO induces XRE-driven luciferase activity in Caco-2 cells. Transfected Caco-2 cells were treated with 0.1 µM, 1 µM, or 3 µM I3MO or 0.1% DMSO as vehicle control for 24 h. Luciferase activity was measured using a secreted luciferase reporter system. Raw luminescence and fluorescence values were corrected by subtracting signals from untransfected cells. Luciferase activity was normalized to fluorescence (Lum/Flu) and expressed as fold change relative to the mean of DMSO-treated controls. Data represent n = 2 independent experiments.

3.2.5 Induction of the endogenous AhR target gene CYP1A1 by FICZ, BaP, I3MO, and I3C

To validate the results obtained from the XRE-driven luciferase reporter assay at the level of endogenous gene expression, quantitative real-time PCR (qPCR) analysis was performed in both cell lines. This approach was used to determine whether the tested compounds are inducing transcription of endogenous AhR target genes in a comparable manner to activating the artificial reporter construct.

For this purpose, the expression of the well-established AhR target genes *CYP1A1* and *TiPARP* were analyzed

The results for *CYP1A1* showed that 3µM I3MO strongly induced its expression in HepG2 cells, displaying the highest level of activation of 400x fold among the tested compounds (Figure 23). In Caco-2 cells, however, the strongest induction of CYP1A1 expression was observed following treatment with 3 µM BaP (Figure 24).
In contrast, I3C induced only weak *CYP1A1* expression in both cell lines and showed the lowest activation levels compared to the other tested ligands, in line with the rather modest activity in the reporter gene assays.

Overall, the induction of *CYP1A1* expression was more pronounced in HepG2 cells than in Caco-2 cells, with expression levels in HepG2 cells being approximately twofold higher under the same experimental conditions.

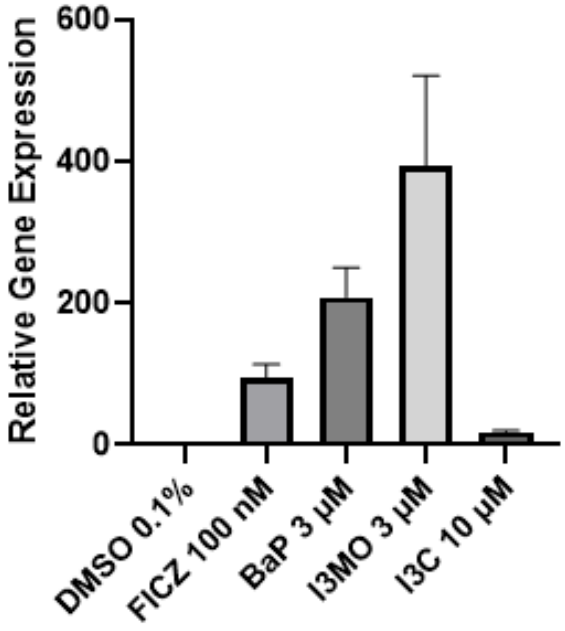

Figure 23 CYP1A1 gene expression in HepG2 cells following treatment with AhR ligands. HepG2 cells were treated with 100 nM FICZ, 3 µM BaP, 3 µM I3MO, 10 µM I3C, or 0.1% DMSO as vehicle control for 24 h. Relative gene expression of CYP1A1 was analyzed by quantitative real-time PCR (qPCR). Ct values were normalized to the housekeeping gene Actin, and relative expression levels were calculated using the $2^{-}\Delta\Delta Ct$ method. Data are presented as fold change relative to the mean of DMSO-treated controls. Data represent n = 2 independent experiments.

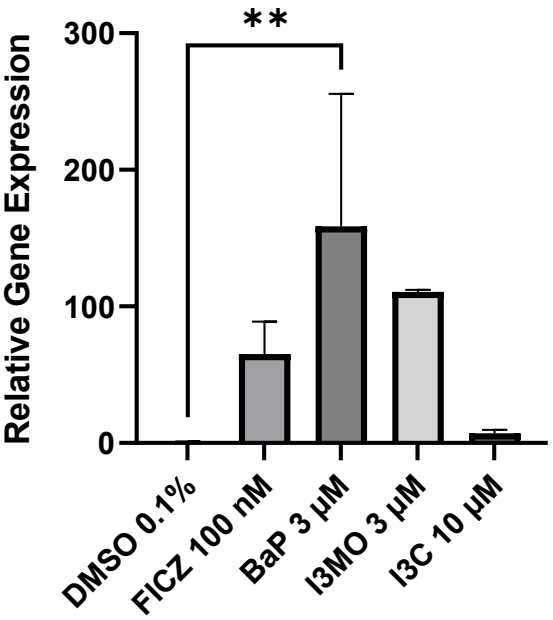

Figure 24 CYP1A1 gene expression in Caco-2 cells following treatment with AhR ligands. Caco-2 cells were treated with 100 nM FICZ, 3 µM BaP, 3 µM I3MO, 10 µM I3C, or 0.1% DMSO as vehicle control for 24 h. Relative gene expression of CYP1A1 was analyzed by quantitative real-time PCR (qPCR). Ct values were normalized to the housekeeping gene Actin, and relative expression levels were calculated using the $2^{-}\Delta\Delta Ct$ method. Data are presented as fold change relative to the mean of DMSO-treated controls. Data represent n = 3 independent experiments.
Statistical significance was determined using one-way ANOVA followed by multiple comparisons test. $p < 0.0001$ vs DMSO. Not significant is not shown.

Concerning *TiPARP* expression, its induction was markedly weaker compared to the activation observed for CYP1A1. In HepG2 cells, treatment with I3MO resulted in the strongest induction of Ti-PARP expression of 2- fold among the tested compounds (Figure 25). In contrast, I3C and FICZ induced only minimal changes in Ti-PARP expression and showed activation levels close to those observed in the DMSO control.

In Caco-2 cells**,** BaP and I3MO produced the strongest induction of *Ti-PARP* expression with approximately 3.5-fold increase over the DMSO control (Figure 26). Treatment with

FICZ resulted in a moderate increase (2- fold) in *Ti-PARP* expression compared to the control. In contrast, I3C induced minimal changes in gene expression, with activation levels similar to those observed for the DMSO control.

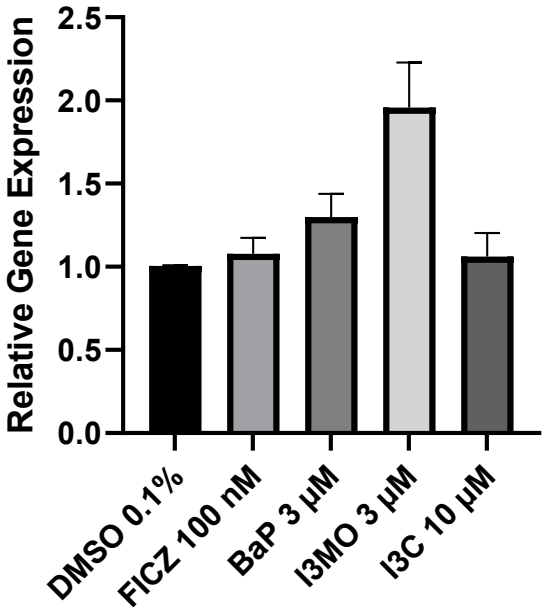

Figure 25 Ti-PARP gene expression in HepG2 cells following treatment with AhR ligands. HepG2 cells were treated with 100 nM FICZ, 3 µM BaP, 3 µM I3MO, 10 µM I3C, or 0.1% DMSO as vehicle control for 24 h. Relative gene expression of CYP1A1 was analyzed by quantitative real-time PCR (qPCR). Ct values were normalized to the housekeeping gene Actin, and relative expression levels were calculated using the $2^{-\Delta\Delta Ct}$ method. Data are presented as fold change relative to the mean of DMSO-treated controls. Data represent n = 2 independent experiments.

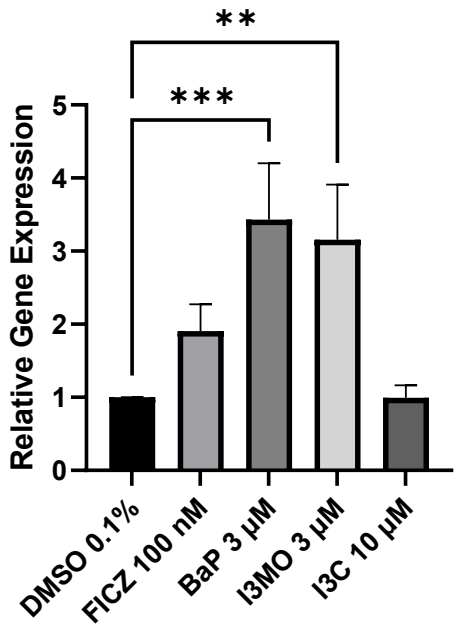

Figure 26 Ti-PARP gene expression in Caco-2 cells following treatment with AhR ligands. Caco-2 cells were treated with 100 nM FICZ, 3 µM BaP, 3 µM I3MO, 10 µM I3C, or 0.1% DMSO as vehicle control for 24 h. Relative gene expression of CYP1A1 was analyzed by quantitative real-time PCR (qPCR). Ct values were normalized to the housekeeping gene Actin, and relative expression levels were calculated using the $2^{-\Delta\Delta Ct}$ method. Data are presented as fold change relative to the mean of DMSO-treated controls. Data represent n = 3 independent experiments.
Statistical significance was determined using one-way ANOVA followed by multiple comparisons test. $p < 0.0001$ vs DMSO. Not significant is not shown.

Overall, the results from the reporter gene assay, where Caco2 cells consistently showed higher luciferase expression and FICZ occurred as the most potent AhR agonist, are not reflected on the level of endogenous target genes. Induction of luciferase from a simplified, plasmid-encoded XRE-driven promoter does not translate one-to-one to the regulation of native target genes, whose expression depends on intricate promoter and enhancer configurations and cell type–specific chromatin and transcription factor landscapes.

3.2.6 Screening project

3.2.6.1 XRE- reporter gene expression in HepG2 treated with gut metabolites

After validation of the XRE reporter gene assay with well-characterized AhR ligands, a panel of different gut-derived metabolites from polyphenols was screened for their potential to activate AhR. The investigated metabolites and their corresponding compound numbers (Compound 1–14) are listed in Table 1. All tested compounds were applied at a final concentration of 30 µM in the wells during the screening experiment.

Since the tested metabolites differed in their solubility, the compounds were dissolved either in water or DMSO and were therefore analyzed in comparison to the respective solvent controls. Accordingly, the screened metabolites were divided into two groups based on their solvent: water-soluble compounds and DMSO-soluble compounds.

Within the group of DMSO-soluble compounds, none of the tested metabolites induced XRE-driven luciferase activity above the levels observed for the DMSO control in either cell line (Figure 27, Figure 28), indicating no detectable AhR activation under the tested conditions. Only compound 13 elicited a two-fold activation in HepG2 cells which was not observed in Caco2 cells.

In contrast, within the group of water-soluble compounds, all tested compounds showed increased XRE reporter activity in both HepG2 and Caco-2 cells during the initial screening (Figure 29, Figure 30), suggesting a general activation of AhR signaling. Notably, Compound 7 and Compound 8 exhibited the strongest induction in both cell lines.

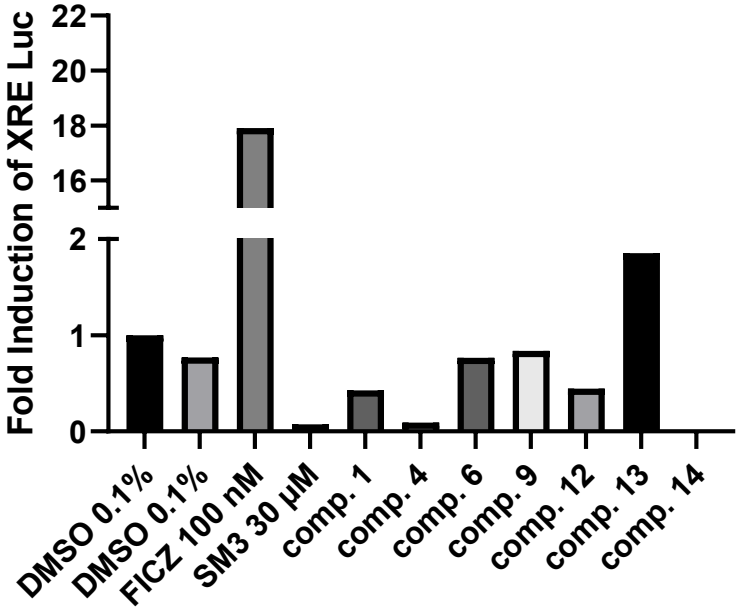

Figure 27 Screening of DMSO-soluble compounds in HepG2 cells using an XRE-driven luciferase reporter assay. Transfected HepG2 cells were treated with 30 µM of each compound or 0.1% DMSO as vehicle control for 24 h. Luciferase activity was measured using a secreted luciferase reporter system. Raw luminescence and fluorescence values were corrected by subtracting signals from untransfected cells. Luciferase activity was normalized to fluorescence (Lum/Flu) and expressed as fold change relative to the mean of DMSO-treated controls. Data represent n = 1 experiment.

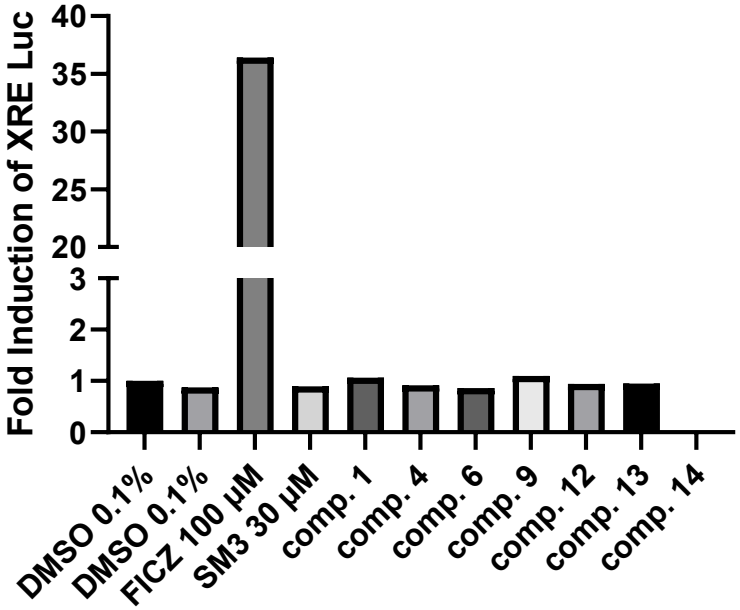

Figure 28 Screening of DMSO-soluble compounds in Caco2 cells using an XRE-driven luciferase reporter assay. Transfected Caco2 cells were treated with 30 µM of each compound or 0.1% DMSO as vehicle control for 24 h. Luciferase activity was measured using a secreted luciferase reporter system. Raw luminescence and fluorescence values were corrected by subtracting signals from untransfected cells. Luciferase activity was normalized to fluorescence (Lum/Flu) and expressed as fold change relative to the mean of DMSO-treated controls. Data represent n = 1 experiment.

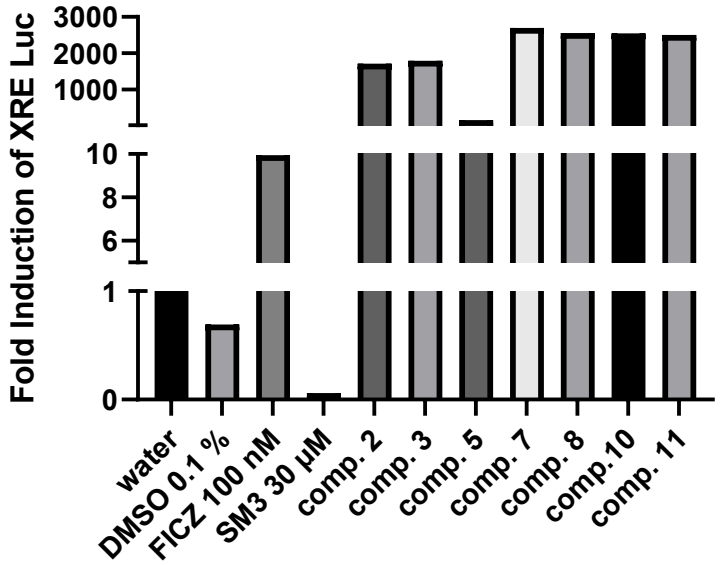

Figure 29 Screening of water-soluble compounds in HepG2 cells using an XRE-driven luciferase reporter assay. Transfected HepG2 cells were treated with 30 µM of each compound or water as vehicle control for 24 h. Luciferase activity was measured using a secreted luciferase reporter system. Raw luminescence and fluorescence values were corrected by subtracting signals from untransfected cells. Luciferase activity was normalized to fluorescence (Lum/Flu) and expressed as fold change relative to the mean of water-treated controls. Data represent n = 1 experiment.

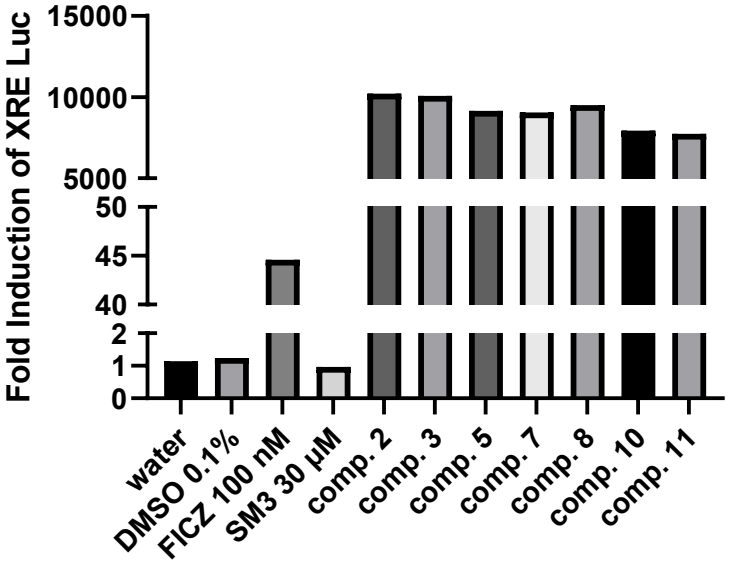

Figure 30 Screening of water-soluble compounds in Caco2 cells using an XRE-driven luciferase reporter assay. Transfected Caco2 cells were treated with 30 µM of each compound or water as vehicle control for 24 h. Luciferase activity was measured using a secreted luciferase reporter system. Raw luminescence and fluorescence values were corrected by subtracting signals from untransfected cells. Luciferase activity was normalized to fluorescence (Lum/Flu) and expressed as fold change relative to the mean of water-treated controls. Data represent n = 1 experiment.

To further investigate whether these compounds induce transcription of endogenous AhR target genes, Compound 7 (vanillin) and Compound 8 (3-hydroxy benzoic acid) were subsequently analyzed in Caco-2 cells using quantitative real-time PCR (qPCR). However, the qPCR analysis did not confirm activation of endogenous AhR target genes. Neither Compound 7 nor Compound 8 induced gene expression levels above those observed in the water-treated control samples (Figure 31, Figure 32). As a positive control, FICZ (100 nM) was included and showed a clear induction of *CYP1A1* expression (Figure 31), whereas induction of *Ti-PARP* was less present and comparable to the levels observed for Compound 7 (Figure 32). These results are consistent with previous reports showing that some gut phenolic metabolites, such as Vanillin and 3-Hydroxybenzoic acid, act as weak or context-dependent AhR modulators. In this assay, they increased XRE-driven luciferase activity, but this was not sufficient to induce endogenous target genes in Caco2 cells, likely due to the higher sensitivity of the reporter system [55].

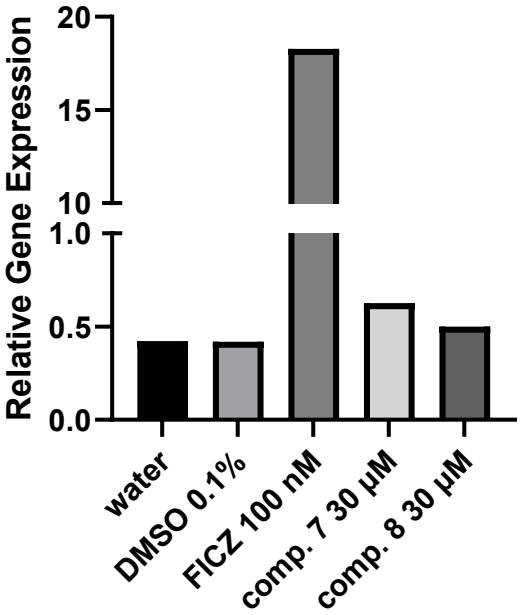

Figure 31 CYP1A1 gene expression in Caco-2 cells following treatment with test compounds. Transfected Caco-2 cells were treated with 30 µM Compound 7, 30 µM Compound 8, 100 nM FICZ as positive control, or 0.1% DMSO as vehicle control for 24 h. Relative gene expression of CYP1A1 was analyzed by quantitative real-time PCR (qPCR). Ct values were normalized to the housekeeping gene Actin, and relative expression levels were calculated using the $2^{-\Delta\Delta Ct}$ method. Data are presented as fold change relative to the mean of DMSO-treated controls. Data represent n = 1 experiment.

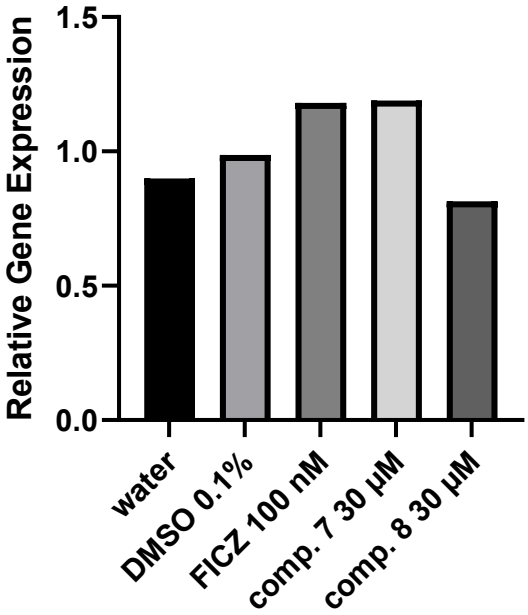

Figure 32 Ti-PARP gene expression in Caco-2 cells following treatment with test compounds. Transfected Caco-2 cells were treated with 30 µM Compound 7, 30 µM Compound 8, 100 nM FICZ as positive control, or 0.1% DMSO as vehicle control for 24 h. Relative gene expression of Ti-PARP (PARP7) was analyzed by quantitative real-time PCR (qPCR). Ct values were normalized to the housekeeping gene Actin, and relative expression levels were calculated using the $2^{-\Delta\Delta Ct}$ method. Data are presented as fold change relative to the mean of DMSO-treated controls. Data represent n = 1 experiment.

Compound number	Metabolite
Compound 1	Protocatechuic acid
Compound 2	Phloroglucinol
Compound 3	3,4-Dihydroxyhydrocinnamic acid
Compound 4	Gallic acid
Compound 5	Hippuric acid
Compound 6	Syringic acid
Compound 7	Vanillin
Compound 8	3-Hydroxybenzoic acid
Compound 9	Vanillic acid
Compound 10	3,4-Dihydroxyphenylacetic acid
Compound 11	3-Hydroxyphenylacetic acid
Compound 12	p-Coumaric acid
Compound 13	3-(3-Hydroxyphenyl)propionic acid
Compound 14	Urolithin A

Table 1 Gut metabolites from phenolics used in this assay

3.2.6.2 XRE- reporter gene expression in HepG2 treated with phyllobilins

Three additional compounds (chlorophyll degradation products from lab of Prof. Simone Moser; SM1–3) were investigated for their potential effects on AhR signaling. From two chemical structures remained elusive, compound 3 was a pheophorbide. They were assessed whether they can modulate AhR-dependent transcriptional activity.

Neither Compound 1 nor Compound 2 induced XRE-driven luciferase activity compared to the DMSO control (Figure 33, Figure 34). Across the tested concentration range, reporter activity remained at basal levels, indicating that both compounds lack agonistic activity toward the AhR under the experimental conditions applied.

In contrast, pheophorbide a exhibited a distinct response pattern (Figure 35). Rather than inducing XRE activation, treatment with this compound resulted in a dose-dependent decrease in the measured XRE-driven reporter activity. The progressive reduction of luciferase signal with increasing concentrations suggests a potential antagonistic effect on AhR signaling. This observation indicates that Pheophorbide a may interfere with AhR-mediated transcriptional activation, although further experiments would be required to confirm its functional role as an AhR antagonist.

The observed decrease in XRE-driven luciferase activity upon treatment with Pheophorbide a was not confirmed at the level of endogenous gene expression, as no corresponding effects were detected in the qPCR analysis.

Notably, pheophorbide a appeared dark in solution, suggesting a potential interference with the luminescence-based readout. Pigmented compounds can absorb or quench emitted light, which may lead to artificially reduced signal intensities in luciferase assays. [56] Importantly, fluorescence values were comparable to those of the 0.1% DMSO control, indicating that cell viability and transfection efficiency were not impaired. Therefore, the reduced reporter activity observed for Pheophorbide a is more likely attributable to optical interference rather than a true inhibition of AhR-mediated transcription.

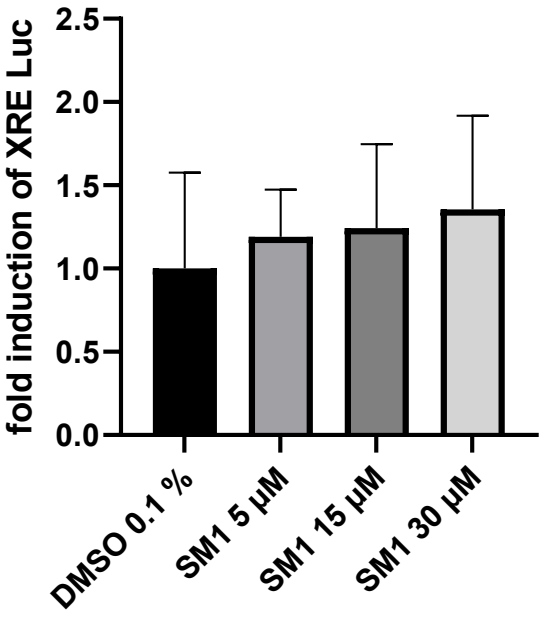

Figure 33 SM1 (Compound 1) does not induce XRE-driven luciferase activity in HepG2 cells. Transfected HepG2 cells were treated with 5 µM, 15 µM, or 30 µM SM1 or 0.1% DMSO as vehicle control for 24 h. Luciferase activity was measured using a secreted luciferase reporter system. Raw luminescence and fluorescence values were corrected by subtracting signals from untransfected cells. Luciferase activity was normalized to fluorescence (Lum/Flu) and expressed as fold change relative to the mean of DMSO-treated controls. Data represent n = 2 independent experiments.

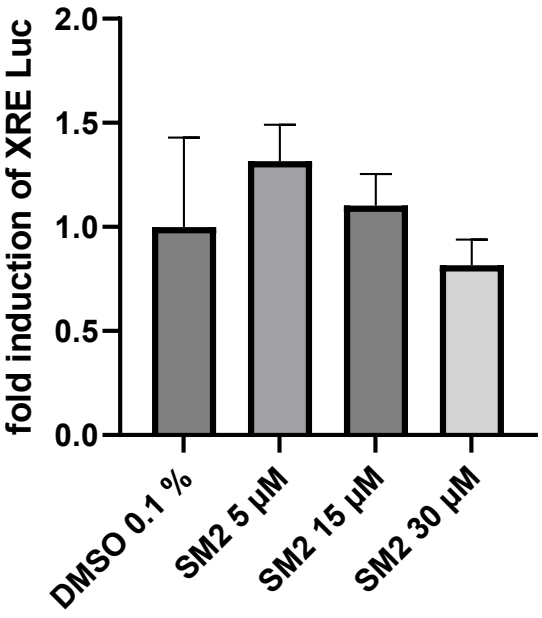

Figure 34 SM2 (Compound 2) does not induce XRE-driven luciferase activity in HepG2 cells. Transfected HepG2 cells were treated with 5 µM, 15 µM, or 30 µM SM2 or 0.1% DMSO as vehicle control for 24 h. Luciferase activity was measured using a secreted luciferase reporter system. Raw luminescence and fluorescence values were corrected by subtracting signals from untransfected cells. Luciferase activity was normalized to fluorescence (Lum/Flu) and expressed as fold change relative to the mean of DMSO-treated controls. Data represent n = 2 independent experiments.

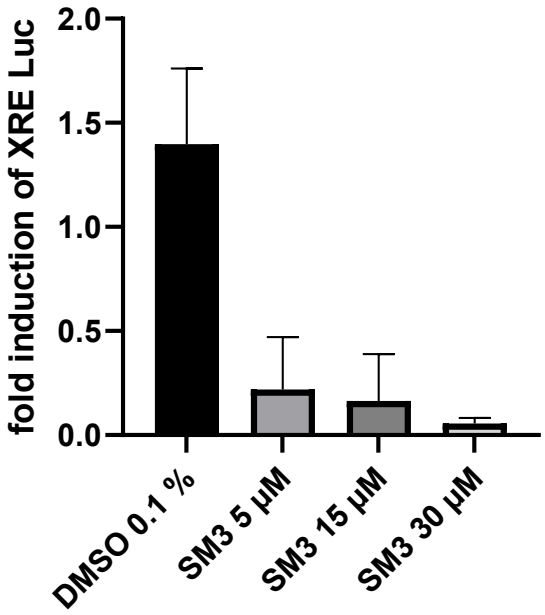

Figure 35 SM3 (Compound 3, Pheophorbide a) reduces XRE-driven luciferase activity in HepG2 cells. Transfected HepG2 cells were treated with 5 µM, 15 µM, or 30 µM SM3 or 0.1% DMSO as vehicle control for 24 h. Luciferase activity was measured using a secreted luciferase reporter system. Raw luminescence and fluorescence values were corrected by subtracting signals from untransfected cells. Luciferase activity was normalized to fluorescence (Lum/Flu) and expressed as fold change relative to the mean of DMSO-treated controls. Data represent n = 2 independent experiments.

3.3 Activation of CLEAR-dependent reporter gene expression in HepG2

3.3.1 Influence of the mTOR Inhibitor Torin1 on CLEAR-driven luciferase expression in HepG2

To evaluate whether inhibition of mTOR signaling affects CLEAR-dependent transcription, transfected cells were treated with increasing concentrations of Torin1, and a CLEAR-driven luciferase reporter assay was performed using either two or four CLEAR elements.

Overall, Torin1 treatment did not result in a dose-dependent increase in luciferase activity for either reporter construct. Across the tested concentrations (50–250 nM), the measured fold induction remained close to or even below the DMSO control, indicating

that Torin1 had no stimulatory or even an inhibitory effect on CLEAR-driven reporter activity under the tested conditions. (Figure 36, Figure 37)

The concentrations used here have been shown in previous studies to inhibit mTORC1 signaling in cell culture, with IC_{50} values in the low nanomolar range [48–50].

Thus, the lack of CLEAR activation cannot be attributed to insufficient mTOR inhibition.

A possible explanation for the lack of CLEAR activation is that mTOR inhibition alone may be insufficient to trigger CLEAR-dependent transcription in these cells. CLEAR activity is known to be modulated by additional factors such as nutrient availability, lysosomal stress, and different post-translational modifications of TFEB [51,52], which could mask a direct response to mTOR inhibition. Furthermore, the duration of Torin1 treatment and the sensitivity of the luciferase reporter could also influence the observed signal.

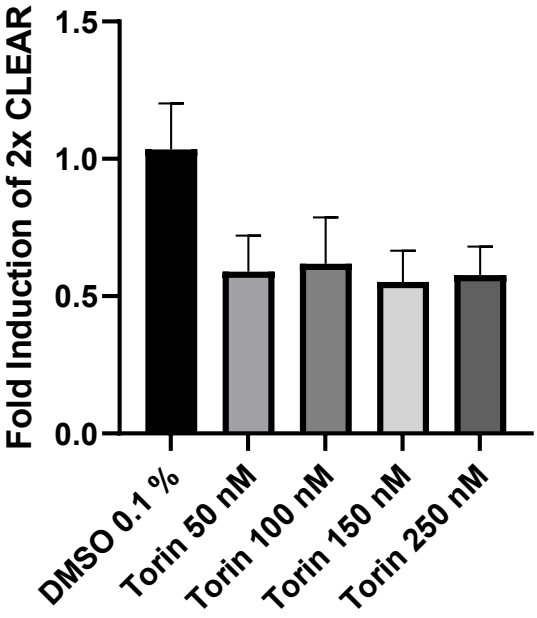

Figure 36 Fold induction of Torin1 in HepG2 cells. HepG2 cells were transiently transfected with a 2× CLEAR luciferase reporter construct and treated with 50 nM, 100 nM, 150 nM, or 250 nM Torin1, or 0.1% DMSO as vehicle control for 24 h. Luciferase activity was measured using a luciferase reporter assay. Raw luminescence and fluorescence values were corrected by subtracting signals from untransfected cells. Luciferase activity was normalized to fluorescence (Lum/Flu) and expressed as fold change relative to the mean of DMSO-treated controls. Data represent n = 2 independent experiments.

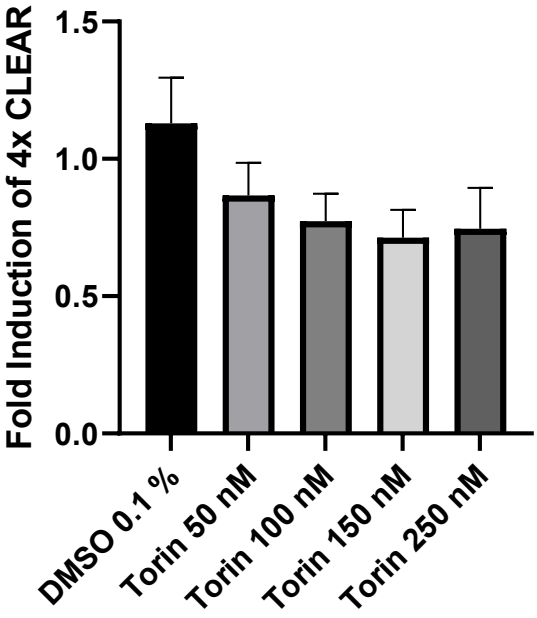

Figure 37 Fold induction of Torin1 in HepG2 cells. HepG2 cells were transiently transfected with a 4× CLEAR luciferase reporter construct and treated with 50 nM, 100 nM, 150 nM, or 250 nM Torin1, or 0.1% DMSO as vehicle control for 24 h. Luciferase activity was measured using a luciferase reporter assay. Raw luminescence and fluorescence values were corrected by subtracting signals from untransfected cells. Luciferase activity was normalized to fluorescence (Lum/Flu) and expressed as fold change relative to the mean of DMSO-treated controls. Data represent n = 2 independent

3.3.2 Influence of a commercially available TFEB-activator on CLEAR-driven luciferase expression in HepG2 cells

To assess the effect of direct TFEB activation on CLEAR-dependent transcription, a CLEAR-driven luciferase reporter assay was performed with increasing concentrations of a commercially available TFEB activator (Figures 38 and 39).
In contrast to the Torin1 experiment, treatment with the TFEB activator resulted in a dose-dependent increase in luciferase activity. While lower concentrations (5–10 µM) showed almost no induction compared to the DMSO control, higher concentrations (15 and 20 µM) led to an increase in CLEAR-driven reporter activity with approximately 3- and 5-fold activation for the 4x CLEAR LUC construct (Figure 39).

Furthermore, the construct containing four CLEAR elements consistently exhibited higher luciferase activity than the construct containing two CLEAR elements. Notably, the signal intensity observed with the 4x CLEAR construct was approximately twofold higher than that of the 2x CLEAR construct under comparable treatment conditions (Figure 39 vs. Figure 38). This difference became particularly evident at higher concentrations of the TFEB activator, suggesting that increasing the number of CLEAR elements enhances the responsiveness of the reporter system.

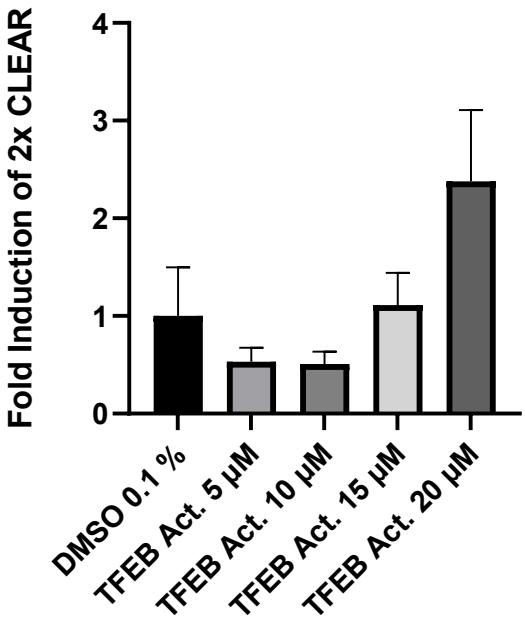

Figure 38 Fold induction of a TFEB activator in HepG2 cells. HepG2 cells were transiently transfected with a 2× CLEAR luciferase reporter construct and treated with 5 µM, 10 µM, 15 µM, or 20 µM TFEB activator, or 0.1% DMSO as vehicle control for 24 h. Luciferase activity was measured using a luciferase reporter assay. Raw luminescence and fluorescence values were corrected by subtracting signals from untransfected cells. Luciferase activity was normalized to fluorescence (Lum/Flu) and expressed as fold change relative to the mean of DMSO-treated controls. Data represent n = 2 independent experiments.

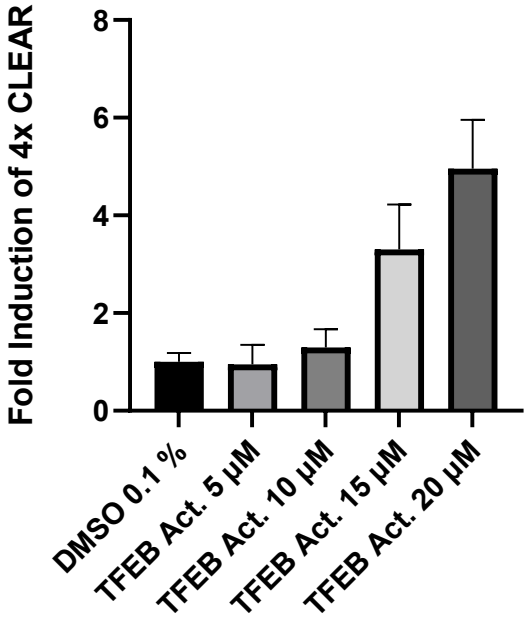

Figure 39 Fold induction of a TFEB activator in HepG2 cells. HepG2 cells were transiently transfected with a 4× CLEAR luciferase reporter construct and treated with 5 µM, 10 µM, 15 µM, or 20 µM TFEB activator, or 0.1% DMSO as vehicle control for 24 h. Luciferase activity was measured using a luciferase reporter assay. Raw luminescence and fluorescence values were corrected by subtracting signals from untransfected cells. Luciferase activity was normalized to fluorescence (Lum/Flu) and expressed as fold change relative to the mean of DMSO-treated controls. Data represent n = 2 independent experiments.

3.3.3 Influence of Thapsigargin on CLEAR-driven luciferase expression in HepG2

Nect, the effect of Thapsigargin, an inhibitor of SERCA,and higher cytosolic calcium levels on Transcription Factor EB (TFEB) activation was examined. Increasing concentrations of Thapsigargin were tested (0.25 µM, 0.5 µM, 1 µM, and 2 µM) using both the 2x CLEAR (Figure 40) and 4x CLEAR (Figure 41) reporter constructs.

In contrast to the TFEB activator experiment, no dose-dependent response was observed. Compared to the DMSO control, luciferase activity was slightly reduced at all tested concentrations. However, one consistent observation was that the 4x CLEAR

construct produced approximately twofold higher luminescence signals than the 2x CLEAR construct under the same conditions, indicating that increasing the number of CLEAR elements enhances the reporter signal even in the absence of a detectable Thapsigargin-induced response.

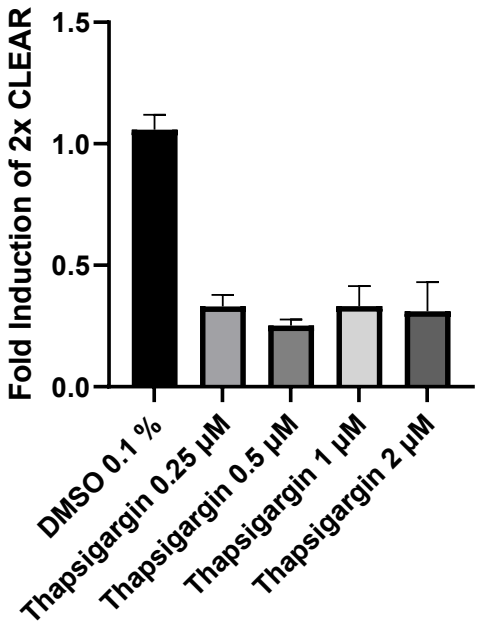

Figure 40 Fold induction of Thapsigargin in HepG2 cells. HepG2 cells were transiently transfected with a 2× CLEAR luciferase reporter construct and treated with 0.25 µM, 0.5 µM, 1 µM, or 2 µM Thapsigargin , or 0.1% DMSO as vehicle control for 24 h. Luciferase activity was measured using a luciferase reporter assay. Raw luminescence and fluorescence values were corrected by subtracting signals from untransfected cells. Luciferase activity was normalized to fluorescence (Lum/Flu) and expressed as fold change relative to the mean of DMSO-treated controls. Data represent n = 1 independent experiments.

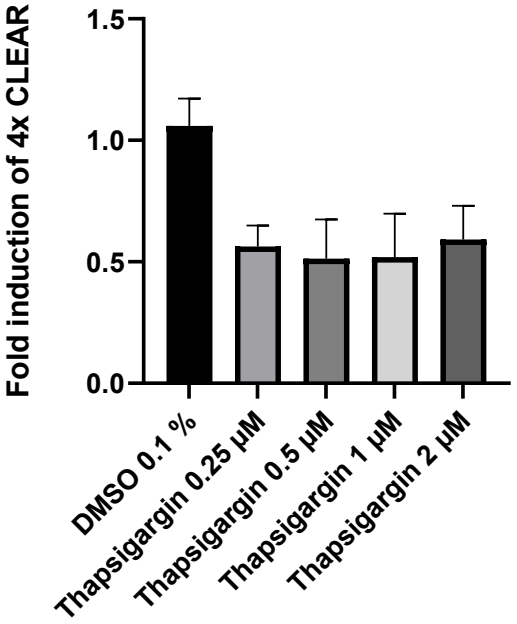

Figure 41 Fold induction of Thapsigargin in HepG2 cells. HepG2 cells were transiently transfected with a 4× CLEAR luciferase reporter construct and treated with 0.25 µM, 0.5 µM, 1 µM, or 2 µM Thapsigargin , or 0.1% DMSO as vehicle control for 24 h. Luciferase activity was measured using a luciferase reporter assay. Raw luminescence and fluorescence values were corrected by subtracting signals from untransfected cells. Luciferase activity was normalized to fluorescence (Lum/Flu) and expressed as fold change relative to the mean of DMSO-treated controls. Data represent n = 1 independent experiments.

3.3.4 Changes in TFEB phosphorylation following Torin1 and Thapsigargin treatment

To investigate whether the treatments affect TFEB activation in HepG2 cells, Western blot analysis was performed using antibodies against total TFEB and phosphorylated TFEB (p-TFEB, serin 211) after 2 h and 6 h of treatment (Figure 46).

Blots probed with a total TFEB antibody showed bands at approximately 65 kDa in torin-treated samples, and at about 70–75 kDa in DMSO- or thapsigargin-treated samples. Because post-translational modifications such as acetylation or phosphorylation can alter gel mobility, the higher–molecular weight band likely represents phosphorylated TFEB, suggesting that torin—but not thapsigargin—reduces TFEB phosphorylation. Consistently, probing for TFEB phosphorylated at serine 211 (an mTORC1-sensitive site) produced no signal in the torin- treated samples and a clear signal after 6 hours of thapsigargin treatment, aligning with inhibited phosphorylation in torin-treated cells and sustained phosphorylation with thapsigargin. However, the absence of any phospho-TFEB signal in DMSO-treated cells remains unexplained.

Overall, these results may suggest that Torin1 treatment leads to a reduction in TFEB phosphorylation over time and should have led to an activation of TFEB dependent transcription, whereas Thapsigargin treatment does not consistently decrease TFEB phosphorylation under the tested conditions. It needs to be noted that the immunoblot was only performed once, calling for caution in data interpretation and conclusions.

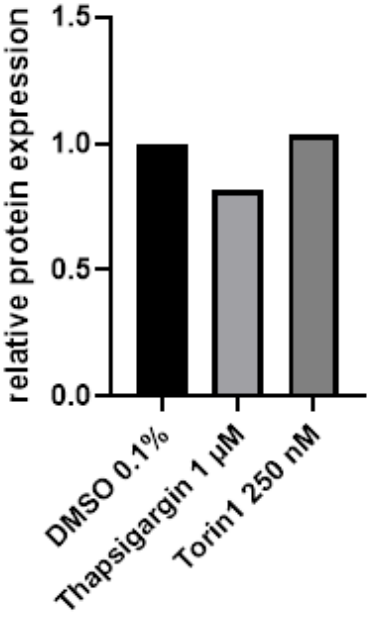

Figure 42 TFEB protein levels in HepG2 cells following treatment with modulators of mTOR signaling. HepG2 cells were treated with 1 µM Thapsigargin, 250 nM Torin1, or 0.1% DMSO as vehicle control for 2 h. Protein expression was analyzed by Western blotting. Membranes were probed with antibodies against TFEB, and Actin was used as a loading control. Band intensities were expressed relative to the DMSO-treated control. Data represent n = 1 experiment.

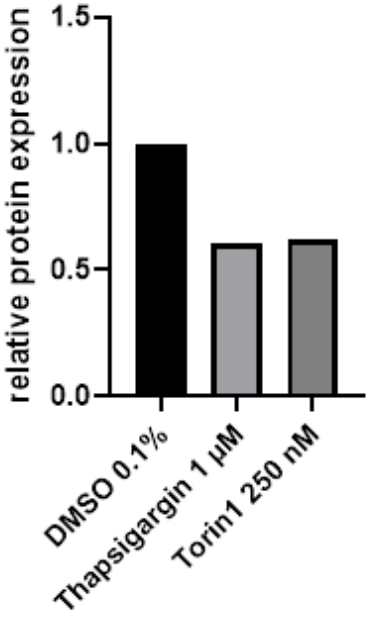

Figure 43 TFEB protein levels in HepG2 cells following treatment with modulators of mTOR signaling. HepG2 cells were treated with 1 µM Thapsigargin, 250 nM Torin1, or 0.1% DMSO as vehicle control for 6 h. Protein expression was analyzed by Western blotting. Membranes were probed with antibodies against TFEB, and Actin was used as a loading control. Band intensities were expressed relative to the DMSO-treated control. Data represent n = 1 experiment.

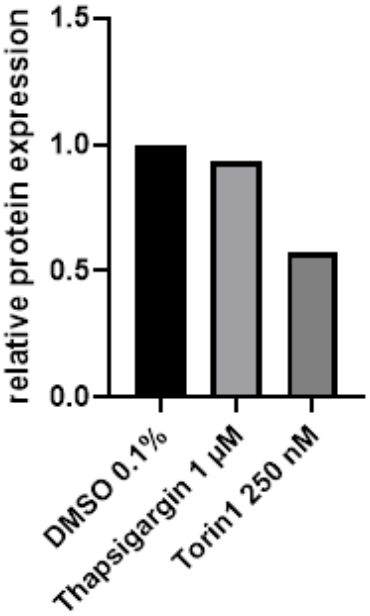

Figure 44 Phosphorylated TFEB (p-TFEB) protein levels in HepG2 cells following treatment with modulators of mTOR signaling. HepG2 cells were treated with 1 µM Thapsigargin, 250 nM Torin1, or 0.1% DMSO as vehicle control for 2 h. Protein expression was analyzed by Western blotting. Membranes were probed with antibodies against phosphorylated TFEB (p-TFEB), and Actin was used as a loading control. Band intensities were expressed relative to the DMSO-treated control. Data represent n = 1 experiment.

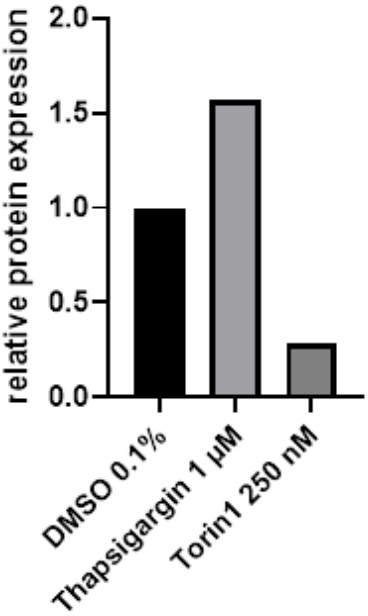

Figure 45 Phosphorylated TFEB (p-TFEB) protein levels in HepG2 cells following treatment with modulators of mTOR signaling. HepG2 cells were treated with 1 µM Thapsigargin, 250 nM Torin1, or 0.1% DMSO as vehicle control for 6 h. Protein expression was analyzed by Western blotting. Membranes were probed with antibodies against phosphorylated TFEB (p-TFEB), and Actin was used as a loading control. Band intensities were expressed relative to the DMSO-treated control. Data represent n = 1 experiment.

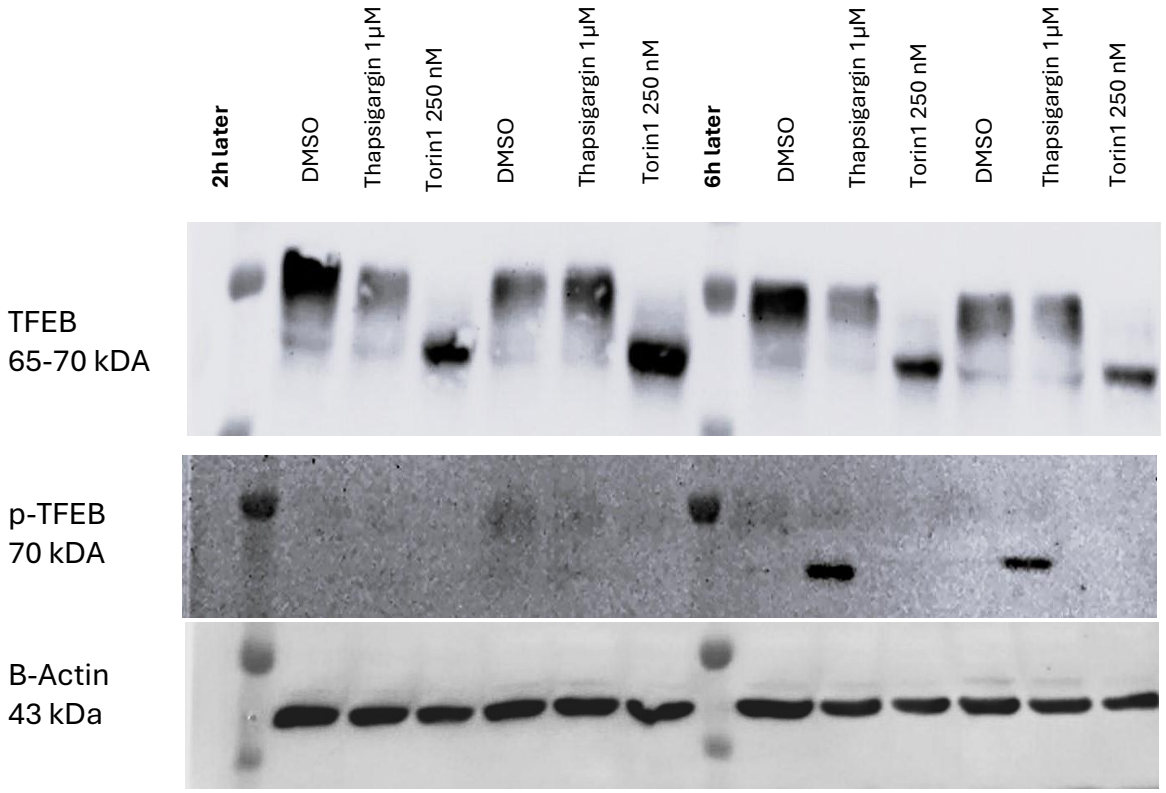

Figure 46-48Western blot membrane showing p-TFEB, total TFEB, and B-ACTIN

4 Conclusion

The aim of this thesis was to establish reporter-based assays for the activity of the cellular transcription factors aryl hydrocarbon receptor (AhR) and transcription factor EB (TFEB). These signaling pathways play a central role in the cellular response to environmental and metabolic stress. The assays developed in this work were designed to provide a reliable platform for future screening approaches aimed at identifying novel modulators of these signaling pathways.

For the AhR pathway, an XRE-driven luciferase reporter assay was successfully established and validated using several compounds previously described in the literature as AhR agonists. All reference compounds tested in this study showed the expected activation of the reporter system, confirming their functionality and suitability as positive controls. Findings from the reporter gene assay were confirmed by induction of endogenous Ahr- dependent target genes, although the extent of induction differed in a gene-, cell type-, and compound-specific manner compared to the reporter assay. These results demonstrate that the established assay reliably detects AhR activation and can serve as a robust basis for future screening projects.

After assay set up, a small-scale screening was performed. Screening of gut-derived metabolites in the reporter assay suggested that all water-soluble compounds activate AhR signaling, with Vanillin (compound 7) and 3-Hydroxybenzoic acid (compound 8) exhibiting the strongest activation in both cell lines. However, subsequent qPCR analysis demonstrated that neither compound induced the expression of the endogenous AhR target genes CYP1A1 and TiPARP. Possible explanations can be that the observed reporter activity for the compounds is an artefact, that the compounds trigger gene selective transcription after activation of AhR, or that off target effects of the compounds interfere with the induction of *CYP1A1* or *TiPARP*. The chlorophyll degradation products SM1 and 2 did not show any effect in the XRE-Luc reporter assay. In contrast, SM3 exhibited a potential antagonistic effect on AhR activity. Nevertheless, additional experiments will be required to determine whether this compound indeed functions as a true AhR antagonist or rather unspecifically decreases the luciferase signal.

For monitoring the TFEB-dependent transcriptional activity, a CLEAR-driven luciferase reporter assay was established. Treatment with the TFEB-activator resulted in a dose-dependent increase in luciferase activity, demonstrating that the reporter construct is capable of detecting TFEB activation. In contrast, treatment with the mTOR inhibitor Torin1 or the SERCA inhibitor Thapsigargin did not produce a comparable dose-dependent response in the luciferase assay, although both perturbations were expected to lead to TFEB activation. One possible explanation may be related to the timing of luciferase measurements (24 hours after treatment), suggesting that further optimization of assay conditions may be required.

To further investigate TFEB regulation, Western blot analysis was performed to assess total TFEB and phosphorylated TFEB (p-TFEB) levels following treatment with Thapsigargin and Torin1. While total TFEB protein levels remained largely unchanged, Torin1 treatment resulted in a reduction of TFEB phosphorylation after 2 and 6 hours treatment, consistent with the inhibition of mTOR signaling and the resulting dephosphorylation of TFEB. In contrast, thapsigargin treatment did not lead to a consistent decrease in p-TFEB levels under the tested conditions. These findings suggest that Torin1 can impede TFEB phosphorylation, but this effect was not clearly reflected in an increased luciferase signal. One explanation, besides the matter of incubation time, could be that Torin-mediated mTOR inhibition markedly shuts down protein translation [57,58] which would be needed for a successful luciferase protein synthesis and luminescence production. However, EGFP levels were only slightly reduced in Torin1-treated samples compared to the DMSO control, suggesting that global protein translation was not markedly impaired under the tested conditions.

Taken together, this study established an AhR reporter assay which represents a useful tool for investigating AhR signaling and for screening of potential pathway modulators. While the TFEB reporter assay showed promising initial results, further optimization will be required to fully capture TFEB-dependent transcriptional responses, , especially when driven by mTOR or Ca-dependent signaling.

5 Material and Methods

5.1 Routinely used Equipment

Consumables	**Provider**
Serological Pipettes (5 ml, 10 ml, 25 ml)	Sarstedt AG & Co. KG (Nümbrecht, Germany)
Pipette tips (10 µL, 200µL, 1000 µL)	Sarstedt AG & Co. KG (Nümbrecht, Germany)
Cell Culture Flask 75 cm2	Sarstedt AG & Co. KG (Nümbrecht, Germany)
CellstarTM 96 Well Cell Culture Plate	Greiner bio-one (Kremsmünster, Austria)
Eppendorf Safe-Lock Tubes 1,5 ml	Eppendorf SE (Hamburg, Germany)

Techniqual Equipment	**Provider**
INTEGRA Pipetboy	INTEGRA Biosciences AG (Zizers, Switzerland)
Eppendorf Pipettes (0,5-10 µl, 2-20 µl, 10-100 µl, 100-1000 µl)	Eppendorf SE (Hamburg, Germany)
VWRTM Analog Vortex Mixer	VWR International GmBH (Randor, PA, USA)
VWRTM Galaxy Mini Microcentrifuge	VWR International GmBH (Randor, PA, USA)
Microsoft® Excel Office 2019	Microsoft Corporation (Redmond, WA, USA)

5.2 Cell culture material and protocols

Techniqual Equipment	Provider
HERAsafe™ KS 18 Workbench	Thermo Fisher Scientific Inc. (Waltham, MA, USA)
HERAcell™ 150 Incubator	Thermo Fisher Scientific Inc. (Waltham, MA, USA)
JULABO™ SW23 Shaking Water Bath	JULABO GmBH (Seelbach, Germany)
Heraeus™ Multifuge™ 1 S-R Centrifuge	Thermo Fisher Scientific Inc. (Waltham, MA, USA)
Olympus CKX41 Microscope	Olympus Optical Co. GmBH (Hamburg, Germany)
Vi-CELL™ XR Cell Viability Analyzer	Beckman Coulter (Brea, CA, USA)
Tecan Spark microplate reader	Tecan Group Ltd., Männedorf, Switzerland

Cell lines	Provider
HEPG2	ATCC
Caco2	Cytion

All cell culture procedures were carried out under aseptic conditions in a laminar airflow cabinet. Cells were maintained in T75 culture flasks containing complete growth medium and incubated at 37 °C in a humidified atmosphere with 5% CO_2.

5.2.1 Passaging

To ensure optimal growth, adherent cells were passaged upon reaching approximately 90% confluence. For both HepG2 and Caco-2 cells, the same general passaging procedure was applied unless stated otherwise. Briefly, the culture medium was aspirated and cells were washed with 10 mL phosphate-buffered saline (PBS). Cells were

subsequently detached using 2 mL trypsin and incubated at 37 °C and 5% CO2 for a maximum of 7 minutes. Enzymatic activity was terminated by addition of serum-containing growth medium. The resulting cell suspension was gently resuspended, transferred to a 50 mL centrifuge tube, and centrifuged at 400 x g for 5 minutes. After removal of the supernatant, the cell pellet was resuspended in fresh complete growth medium.

HepG2 cells were routinely subcultivated at a split ratio of 1:10 at the beginning of the week, 1:5 on Thursdays or Fridays, depending on the confluence of the cells and seeded into new T75 culture flasks with a final volume of 10 mL complete growth medium.

For Caco-2 cells, a defined seeding strategy was employed to maintain the cells in an undifferentiated state. On Mondays 1.0×10^6 cells were seeded into a new T75 flask. On Fridays, 1.0×10^6 cells were distributed into a T75 flask (2 flasks). Passaging on Fridays involved transfer into two T75 flasks. The final culture volume for Caco-2 cells was adjusted to 15 mL per flask.

Materials	**Components**	**Amount**	**Source**
PBS (phosphate buffered saline) pH 7.4	NaCl Na_2HPO_4 KH_2PO_4 ddH_2O	36.0 g 7.4 g 2.15 g	Carl Roth (Karlsruhe, DE)
Trypsin	Trypsin Na_2EDTA PBS	0.05 % 0.02 % 1000 ml	Gibco (Lofer, AT) Gibco (Lofer, AT)
Complete growth medium (for HepG2)	EMEM (500 ml) Heat-inactivated FBS L-Glutamine 2 mM Penicillin - Streptomycin	500 ml 10 % 1% 1%	Sigma-Aldrich (St. Louis, US) Gibco (Lofer, AT) Lonza (Basel, CH) Lonza (Basel, CH)
Complete growth medium (for CaCo2)	EMEM (500 ml) Heat-inactivated FBS L-Glutamine 2 mM Penicillin–Streptomycin Non-essential amino acids (NEAA)	500 ml 20 % 1 % 1 % 1x	Sigma-Aldrich (St. Louis, US) Gibco (Lofer, AT) Lonza (Basel, CH) Lonza (Basel, CH)

5.3 Luciferase reporter gene assay

Used Items

Consumables	Provider
Pipette tips (10 µl, 200 µl, 1000 µl)	Sarstedt AG & Co. KG (Nümbrecht, Germany)
Eppendorf Safe-Lock Tubes 1,5 ml	Eppendorf SE (Hamburg, Germany)
Serological pipettes (5 ml, 10 ml, 25 ml)	Sarstedt AG & Co. KG (Nümbrecht, Germany)

Technical Equipment	Provider
Eppendorf Pipettes (0,1-2,5 µl, 0,5-10 µl, 2- 20 µl, 10-100 µl, 100-1000 µl)	Eppendorf SE (Hamburg, Germany)
INTEGRA Pipetboy	INTEGRA Biosciences AG (Zizers, Switzerland)
VWR™ Analog Vortex Mixer	VWR International GmBH (Randor, PA, USA)
VWR™Galaxy Mini Microcentrifuge	VWR International GmBH (Randor, PA, USA)
Microsoft® Excel Office 2019	Microsoft Corporation (Redmond, WA, USA)

5.3.1 Principle of Aryl Hydrocarbon receptor assay

The luciferase reporter gene assay was used to evaluate transcriptional activation of the aryl hydrocarbon receptor (AhR) signalling pathway. Cells were transiently transfected using Lipofectamine® and P3000™ with a reporter plasmid containing a xenobiotic response element (XRE) upstream of a gene encoding a secreted Nanoluciferase. Activation of the AhR pathway by test compounds resulted in binding of AhR to the XRE and induction of luciferase gene expression

The expressed luciferase was secreted into the cell culture supernatant where quantified using the Nano-Glo® Luciferase Assay System (Promega). Upon addition of the Nano-Glo® substrate, a luminescent signal was generated, which was measured with the luminescence mode in the TECAN Spark. Luminescence intensity directly reflected XRE-driven transcriptional activity and was used to assess the activation of the AhR pathway by the tested compounds.

5.3.1.1 Splitting and Seeding of HEPG2 and Caco2 cells into dishes

On Monday, HepG2 and Caco-2 cells were split and seeded into 96-well plates at a density of 30.000 cells per well in a final volume of 100 µL culture medium per well.

5.3.1.2 Transfection via Lipofectamine® and P3000™

Approximately 24 hours after seeding, transient transfection was performed using the Lipofectamine® reagent in combination with P3000™ (Thermo Fisher Scientific) according to the manufacturer´s instructions. Cells were transfected with a reporter plasmid containing a xenobiotic response element (XRE) upstream of a gene encoding a secreted luciferase, together with a plasmid encoding enhanced green fluorescent protein (EGFP) to monitor transfection efficiency and cell viability.

Two separate mixtures were prepared for the transfection. Tube 1 contained 5 µL Opti-MEM® and 0.15 µL Lipofectamine®. Tube 2 contained 100 ng total DNA (75 ng XRE-luciferase reporter plasmid and 25 ng EGFP plasmid) and 0.2 µL P3000™ reagent (amounts and volumes for one well). The contents of tube 2 were added to tube 1, gently mixed, and incubated for 15 minutes at room temperature to allow formation of DNA-lipid complexes. The DNA-containing transfection mixture was prepared in bulk as a master mix for 100 wells.

Subsequently, 10 µL of the transfection complex were added to each well of a 96 well plate containing cells in culture medium. Cells were incubated under standard culture conditions. Wells in column A served as non-transfected controls and received a control mixture containing Lipofectamine®, Opti-MEM®, and P3000™, but no plasmid DNA, which was prepared in bulk for 10 wells. The detailed pipetting scheme and exact volumes per well are provided in Table 2.

	Opti-MEM	Lipofectamine	P3000™	g DNA
Untransfected Tube A	50 µL	0.75 µL		
Untransfected Tube B	50 µL		2 µL	
Transfected Tube A	50 µL	0.75 µL		
Transfected Tube B	500 µL		2 µL	1 µg (0.25 µG EGFP + 0.75 µg Plasmid DNA)

Table 2 pipetting scheme

5.3.1.3 Change medium

24 hours after the transfection it is necessary to remove any luciferase that had already been secreted under basal conditions and to ensure that subsequent measurements reflected only the effect of the test compounds. Therefore, the old culture medium was replaced with fresh medium (100 µL per well) prior to compound treatment.

5.3.1.4 Compound treatment

Compounds were prepared as 1000x stock solutions in DMSO corresponding to 1000 times the intended final working concentration and stored at −20 °C in aliquots. On the day of treatment, stock solutions were thawed at room temperature and briefly vortexed to ensure homogeneity. For compound application, 2 µL of the 1000x stock solution were added to 1 mL of pre-warmed culture medium of the respective cell type and vortexed thoroughly. From this dilution, 100 µL were transferred to each well of a 96-well plate already containing 100 µL of culture medium with cells, resulting in a final volume of 200

µL per well. Control wells received the corresponding amount of DMSO diluted in culture medium. Plates were gently swirled to ensure even distribution of the compounds and incubated under standard culture conditions (37 °C, 5 % CO_2).

5.3.1.5 Measurement

The 96-well plate was removed from the incubator 24 hours after compound treatment and from each well, 50 µL of supernatant containing the secreted luciferase was transferred to a new white 96-well plate.

The Nano-Glo® Luciferase Assay Reagent was freshly prepared by mixing Nano-Glo® Luciferase Assay Substrate with Nano-Glo® Luciferase Assay Buffer at a ratio of 1:50. The reagent was prepared using 5,250 µL buffer and 105 µL substrate for one 96-well plate. Subsequently, 50 µL of the prepared Nano-Glo® reagent was added to each well of the white plate. Luminescence was measured using a Tecan Spark microplate reader,

Following luminescence measurement, the remaining medium was removed from the original cell culture plate, which was then stored at −80 °C for subsequent enhanced green fluorescent protein (eGFP) analysis.

2 hours later, the frozen cell culture plate was removed from the freezer and allowed to thaw at room temperature. Subsequently, 100 µL of NPLC lysis buffer was added to each well, and the plate was shaken for 10 minutes to ensure complete cell lysis. Thereafter, 50 µL from each well was transferred to a black 96-well plate. Fluorescence was measured using the Tecan Spark microplate reader in GFP fluorescence mode.

Material	**Components**	**Amount**	**Source**
NPLC buffer	NaCl	4.39 g	Carl Roth (Karlsruhe, DE)
	HEPES (free acid)	5.96 g	Carl Roth (Karlsruhe, DE)
	NaOH	Adjusted to pH 7.4	Carl Roth (Karlsruhe, DE)
	ddH20	to 500 ml	

Material	**Amount**	**Source**
Buffer	5.250 µL	Promega (Madison, US)
Reagent	105 µL	Promega (Madison, US)

5.3.1.6 Data analysis

The experiments were conducted in four technical replicates per condition, and data analysis was performed using Microsoft Excel. Luminescence values from transfected wells were background-corrected by subtracting the mean signal obtained from untransfected control wells. The same background correction procedure was applied to the corresponding fluorescence values. To normalize luciferase activity to transfected cell number, the corrected luminescence values were divided by the corrected fluorescence values for each well. The resulting normalized values were then expressed as fold change relative to the mean of the DMSO-treated control group, which was set to 1.0.

5.3.2 Principle of transcription factor EB assay

The CLEAR- driven luciferase reporter gene assay was used to evaluate transcriptional activation mediated by transcription factor EB (TFEB). Cells were transiently transfected using Lipofectamine® and P3000™ with luciferase reporter plasmids containing either two or four copies of the Coordinated Lysosomal Expression and Regulation (CLEAR) element upstream of a gene encoding intracellular firefly luciferase. Activation of TFEB by test compounds resulted in binding of TFEB to the CLEAR elements and induction of intracellular firefly luciferase gene expression.

The expressed luciferase was quantified after cell lysis. Upon addition of the luciferase substrate using the injector system of a Tecan plate reader, a luminescent signal was generated and measured. Luminescence intensity directly reflected CLEAR-driven transcriptional activity and was used to assess activation of TFEB by the tested compounds.

5.3.2.1 Splitting and Seeding of HepG2 cells into dishes

On Monday, HepG2 cells were split and seeded into 96-well plates at a density of 30.000 cells per well in a final volume of 100 µL culture medium per well.

5.3.3.2 Transfection via Lipofectamine® and P3000™

Approximately 24 hours after seeding, transient transfection was performed using the Lipofectamine® reagent in combination with P3000™ (Thermo Fisher Scientific) according to the manufacturer's instructions. Cells were transfected with luciferase reporter plasmids containing CLEAR elements upstream of a gene encoding luciferase, together with a plasmid encoding enhanced green fluorescent protein (EGFP) to monitor transfection efficiency and cell viability.

Two separate mixtures were prepared for transfection. For one well, tube A contained 5 µL Opti-MEM® and 0.15 µL Lipofectamine®. Tube B contained 5 µL Opti-MEM®, 100 ng total DNA, and 0.2 µL P3000™ reagent. For one half of the plate, the DNA mixture consisted of 75 ng pGL2 luciferase plasmid and 25 ng EGFP plasmid per well, whereas the other half of the plate was transfected with 75 ng CLEAR-Luc 4× reporter plasmid and 25 ng EGFP plasmid per well. The DNA-containing transfection mixtures were prepared in bulk for 50 wells each. The contents of tube B were added to tube A, gently mixed, and incubated for 15 minutes at room temperature to allow formation of DNA–lipid complexes.

Subsequently, 10 µL of the transfection complex were added to each well of a 96-well plate containing cells in culture medium. Cells were incubated under standard culture conditions. Wells designated as non-transfected controls received a control mixture containing Lipofectamine®, Opti-MEM®, and P3000™, but no plasmid DNA, which was prepared in bulk for 10 wells.

5.3.2.3 Compound treatment

Compounds were prepared as 1000x stock solutions in DMSO corresponding to 1000 times the intended final working concentration and stored at −20 °C in aliquots. On the day of treatment, stock solutions were thawed at room temperature and briefly vortexed to ensure homogeneity. For compound application, 2 µL of the 1000x stock solution were added to 1 mL of pre-warmed culture medium of the respective cell type and vortexed thoroughly. From this dilution, 100 µL were transferred to each well of a 96-well plate containing 100 µL of culture medium with cells, resulting in a final volume of 200 µL per well. Control wells received the corresponding amount of DMSO diluted in culture

medium. Plates were gently swirled to ensure even distribution of the compounds and incubated under standard culture conditions (37 °C, 5 % CO_2).

5.3.2.4 Measurement

For measurement of the TFEB luciferase reporter gene assay, the 96-well plate was removed from the incubator 24 hours after compound treatment. The culture medium was completely removed from each well, and the plate was stored at −80 °C for at least 1 hour to facilitate subsequent cell lysis.

During the freezing period the luciferin and ATP solutions were thawed, the lysis buffer was freshly prepared, and the injector system of the Tecan Spark microplate reader was washed, primed, and backflushed with water and ethanol.

Material	Components	Amount	Source
Luciferase lysis buffer	ddH_2O	4.8 ml	
	5x lysis buffer	1.2 ml	Promega(Madison,US)
	CoA (270 mM)	2 µl	Sigma Aldrich(St.Louis, US)
	DTT (1 M)	2 µl	Fluka (Buchs, CH)

After 1 hour, the plate was removed from the freezer and allowed to thaw at room temperature. Subsequently, 50 µL of lysis buffer were added to each well, and the plate was shaken for 10 minutes to ensure complete cell lysis. Thereafter, 40 µL of the cell lysate from each well were transferred to a black 96-well plate.

Prior to measurement, the ATP solution was loaded into injector A and the luciferin solution into injector B of the Tecan Spark microplate reader, followed by priming of both injectors. Fluorescence was measured first to determine EGFP signal, after which luciferase activity was quantified by luminescence measurement in each well.

Material	Components	Source
ATP	Tricine pH 7.8 (2 mM) $MgCl_2$ (21.5 mM) ATP (3.8 mM)	Sigma-aldrich (St. Louis, US)

Luciferin	Luciferin (32 mg/ml) Tricine pH 7.8 (21 mM)	Synchem (Elk grove Village, US)

5.3.2.5 Data analysis

Experiments were performed with four technical replicates per condition, and data were analyzed using Microsoft Excel. Luminescence values from transfected wells were first corrected for background by subtracting the mean signal obtained from untransfected control wells. The same background correction was applied to the corresponding fluorescence values. To account for differences in cell number, the background-corrected luminescence values were divided by the background-corrected fluorescence values for each well. The resulting normalized values were then expressed as fold change relative to the mean of the DMSO-treated or medium-only control group, which was set to 1.0.

5.4 Plasmid amplification in bacteria

Consumables	**Provider**
Serological Pipettes (5 ml, 10 ml, 25 ml)	Sarstedt AG & Co. KG (Nümbrecht, Germany)

Technical Equipment

Name	**Provider**
MaxQTM 4000 Benchtop Orbital Shaker	Thermo Fisher Scientific Inc. (Waltham, MA, USA)
Sorvall® RC-5C Plus Superspeed Centrifuge	Kendro Laboratory Products (Newtown, CT, USA)
NanoDropTM 2000c Spectrophotometer	Thermo Fisher Scientific Inc. (Waltham, MA, USA)
INTEGRA Pipetboy	INTEGRA Biosciences AG (Zizers, Switzerland)

Media, solutions and reagents

Name	**Components**	**Provider**
LB-Media (Lennox)		Carl Roth (Karlsruhe, Germany)
Ampicillin sodium salt		Carl Roth (Karlsruhe, Germany)
PureLink™ HiPure Plasmid Midiprep Kit	Resuspension Buffer (R3) RNase A Lysis Buffer (L7) Precipitation Buffer (N3) Equilibration Buffer (EQ1) Wash Buffer (W8) Elution Buffer (E4) TE Buffer HiPure Columns Column Holders	Thermo Fisher Scientific Inc. (Waltham, MA, USA)

Plasmids used in this work

Plasmid Name	Addgene Plasmid	Bacterial Resistances	Source
XRE-pNL1.3[secNLuc]	#182295	Ampicillin 100 µg/mL	Addgene (Watertown, MA, USA)
pGL2-2xCLEAR-luciferase	#81120	Ampicillin 100 µg/mL	Addgene (Watertown, MA, USA)
4xCLEAR-luciferase reporter	#66800	Ampicillin 50 µg/mL	Addgene (Watertown, MA, USA)

5.4.1 Midi Prep starting

To amplify the plasmid, 500 mL LB medium was prewarmed prior to use. The bacterial stock, stored at -70°C in glycerol, was thawed on ice. The prewarmed LB medium was transferred into a large Erlenmeyer flask and Ampicillin was added to LB medium at a final concentration of 100 or 50 µg/mL. Subsequently, 50 µL of the thawed bacterial stock was inoculated into the medium. The culture was then incubated overnight on a shaker at 180 rpm and 37 °C to allow for bacterial growth. This overnight culture served as the starting material for subsequent plasmid isolation using a midi-prep procedure.

5.4.2 Plasmid isolation

Before starting the plasmid isolation, it was ensured that RNase A was included in the Resuspension Buffer (R3). The Lysis Buffer (L7) was briefly warmed to 37 °C to dissolve any particulate matter. The column was prepared by applying 10 mL of Equilibration Buffer (EQ1) and allowing it to drain by gravity.

The overnight LB bacterial culture was harvested by centrifugation at 4,000 × g for 10 minutes and the supernatant medium was completely removed. The resulting cell pellet was resuspended in 4 mL of cold Resuspension Buffer (R3) containing RNase A until a homogeneous suspension was obtained. Subsequently, 4 mL of Lysis Buffer (L7) were added, and the mixture was gently inverted until fully homogeneous. The lysate was incubated at room temperature for 5 minutes before being transferred to a separate tube.

Following lysis, 4 mL of Precipitation Buffer (N3) were added, and the mixture was immediately inverted until homogeneous. The sample was centrifuged at over 17,000 × g for 20 minutes at room temperature to remove cellular debris. The clarified supernatant was then applied to the pre-equilibrated column and allowed to pass through by gravity. The column was washed twice with 10 mL of Wash Buffer (W8), discarding the flow-through after each wash.

For DNA elution, a sterile 15 mL centrifuge tube was placed under the column, and 5 mL of Elution Buffer (E4) were added, allowing the purified DNA to flow into the tube. To precipitate the DNA, 3.5 mL of ice-cold isopropanol were added to the eluate and mixed thoroughly, followed by centrifugation at over 12,000 × g for 30 minutes at 4 °C. The supernatant was carefully removed, and the DNA pellet was washed with 3 mL of 70 % ethanol and centrifuged again at the same speed for 5 minutes at 4 °C. After discarding the supernatant, the pellet was air-dried for at least 10 minutes and initially resuspended in 40 µL of TE buffer. Depending on the downstream application, the solution was further diluted. The concentration of the purified plasmid DNA was subsequently determined using a NanoDrop™ 2000c spectrophotometer. The isolated plasmid DNA was then stored at - 20° C.

5.5 Protein extraction, SDS PAGE and Western Blot

Consumables	**Provider**
Gel Loading Pipet Tips 1-200 µL	Thermo Fisher Scientific Inc. (Waltham, MA, USA)
AmershamTM HybondTM PVDF membrane	Cytiva (Malborough, MA, USA)

Technical Equipment	Provider
SONOPLUS ultrasonic homogenizer HD 2070	Bandelin (Berlin, Germany)
HeraeusTM Biofuge™ fresco Microcentrifuge	Thermo Fisher Scientific Inc. (Waltham, MA, USA)

Tecan Sunrise™ Plate Reader	Tecan Group (Männedorf, Switzerland)
IKA® Vibrax® VXR basic Shaker	IKA Werke (Staufen, Germany)
Dry Block Heating System QBD2	Grant (Cambridge, UK)
PowerPac™ HC power supply	BIO-RAD Laboratories (Hercules, CA, USA)
PowerPAC BASIC™ power supply	BIO-RAD Laboratories (Hercules, CA, USA)
Mini-PROTEAN® 3 Cell	BIO-RAD Laboratories (Hercules, CA, USA)
Mini PROTEAN® Tetra Cell	BIO-RAD Laboratories (Hercules, CA, USA)
Mini Trans-Blot® Electrophoretic Transfer Cell	BIO-RAD Laboratories (Hercules, CA, USA)
Amersham™ ImageQuantTM 800 Western blot imaging systems	Cytiva (Malborough, MA, USA)
ImageQuant™ TL Software	Cytiva (Malborough, MA, USA)
GraphPad Prism 9 Software	GraphPad Software, Inc. (Boston, MA, USA)

Solutions and reagents

Name	**Provider**
Precision Plus ProteinTM Standard All Blue	BIO-RAD Laboratories (Hercules, CA, USA)

Name	**Ingridients**	
RIPA buffer	NaCl 150 mM	483.3 mg
	Tris-HCl 50 mM	394.0 mg
	Nonidet P 40	500,0 mg
		125.0 mg
		50.0 mg

	Deoxycholic acid sodium salt	
	SDS	
Lysis Buffer	RIPA buffer	1410 µL
	Complete	60 µL
	PMSF 0.1 M	15 µL
	NaF 200 mM	7.5 µL
	Na3VO4 200 mM	7.5 µL
Bradford Solution	ROTI®-Quant (Carl Roth, Karlsruhe, Germany)	200 µL
	H2O dd	Ad 1000 µL
Separation Gel 7,5 % (2 Gels)	30 % PAA 1,5 M	3.75 mL
	Tris-HCl pH 8,8	3.75 mL
	10 % SDS	150 µL
	H2O dd	7.35 mL
	TEMED	15 µL
	APS 10 %	75 µL
Stacking Gel (2 Gels)	30 % PAA	1.28 mL
	1,25 M Tris-HCl pH 6,8	750 µL
	10 % SDS	75 µL
	H2O dd	5.25 mL
	TEMED	15 µL
	APS 10 %	75 µL
3X SDS-PAGE Loading buffer	0.5 M Tris- HCl pH 6.8	37.5 mL
	SDS	6.0 g
	Glycerol	30.0 ml
	Bromphenol blue	15.0 mg
	H20 dd	Ad 100 mL
Elektrophoresis buffer (10X)	Tris-Base	30 g
	Glycine	144 g
	SDS	10 g
	H20 dd	Ad 1000 ml

Blotting Buffer (5X)	Tris- Base	15.169 g
	Glycine	72.9 g
	H20 dd	Ad 1000 mL
Blocking Solution with 5 % BSA	Bovine Serum Albumin (Carl Roth Karlsruhe, Germany)	5.0 g
	TBS-T	Ad 100 mL
Milk Solution	Milk powder	5.0 g
	H20 dd	Ad 100 ml

Antibody	**Catalogue number**	**Species**	**Dilution**	**Provider**
β-Actin	8457	mouse	1:1000	Cell Signaling Technology Europe B.V. (Frankfurt am Main, Germany)
p-TFEB	37681	rabbit	1:1000	Cell Signaling Technology Europe B.V. (Frankfurt am Main, Germany)
TFEB	4240	rabbit	1:1000	Cell Signaling Technology Europe B.V. (Frankfurt am Main, Germany)
Anti-rabbit IgG, HRP-linked Antibody		goat	1:15000	Cell Signaling Technology Europe B.V. (Frankfurt am Main, Germany)

Anti-mouse IgG, HRP-linked Antibody	goat	1:15000	Cell Signaling Technology Europe B.V. (Frankfurt am Main, Germany)

5.5.1 Cell lysis

A fresh lysis buffer was prepared for protein extraction by combining 1,410 µL RIPA buffer, 60 µL Complete protease inhibitor, 15 µL 0.1 M PMSF, 7.5 µL 200 mM NaF, and 7.5 µL 200 mM Na_3VO_4. Cells were lysed by adding 100 µL of this buffer per well, followed by incubation on ice for 10 minutes. Cells were then scraped, and the lysates were transferred into microcentrifuge tubes.

To ensure complete cell disruption, samples were sonicated for 10 seconds and subsequently centrifuged at 4 °C for 20 minutes. After centrifugation, the supernatant containing soluble proteins was carefully collected, while the pellet was discarded. From the supernatant, 80 µL were transferred into 1.5 mL tubes for SDS-PAGE sample preparation. In addition, 5 µL were transferred into separate tubes and diluted with 45 µL ddH_2O on ice for subsequent protein quantification.

A denaturation mixture for SDS-PAGE was prepared by mixing sample buffer (SP) and β-mercaptoethanol (765 µL SP buffer and 135 µL β-mercaptoethanol). 40 µL of this mixture were added to each lysate sample. Samples were heated at 95 °C for 10 minutes to ensure complete protein denaturation. After incubation, the denatured lysates were stored at −20 °C until further analysis.

5.5.2 Protein quantification

Protein concentrations were determined using the Bradford assay to ensure equal protein loading for subsequent SDS-PAGE. For this purpose, lysates were diluted 1:10

with ddH_2O, and 10 µL of each dilution were pipetted in triplicates into a 96-well plate. To generate a standard curve, bovine serum albumin (BSA) standards ranging from 0 to 500 µg/mL were also loaded in triplicates on the same plate. Protein standards were placed in columns 1–3, while samples were loaded in columns 4–9.

Each standard well received 5 µL of 1:10 diluted lysis buffer and 10 µL of the respective standard solution, whereas sample wells were loaded with 10 µL ddH_2O followed by 5 µL of diluted lysate. The Bradford reagent was diluted 1:5 with ddH_2O, and 190 µL were added to each well. After incubation at room temperature for 5 minutes, absorbance was measured at 595 nm using a SUNRISE microplate reader (Tecan Group Ltd., Männedorf, Switzerland) following a brief 5-second shaking step.

Protein concentrations were determined using the Bradford method, which is based on the binding of Coomassie Brilliant Blue dye to proteins, resulting in an absorbance shift at 595 nm. Sample concentrations were calculated by comparison to a standard calibration curve generated with known protein standards.

5.5.3 SDS- PAGE

Sodium dodecyl sulfate polyacrylamide gel electrophoresis (SDS-PAGE) was performed to separate proteins according to their molecular weight. Separation is achieved by denaturing the proteins and coating them with SDS, which imparts a uniform negative charge so that migration through the gel depends primarily on protein size.

Polyacrylamide gels were prepared the evening before use. The percentage of the separation gel (7.5–10 %) was chosen based on the sizes of the target proteins (see Table 18). Gels were poured into a casting frame between two glass plates, overlaid with 1 mL of ddH_2O to prevent evaporation, and allowed to polymerize for 1 hour. After removal of the water, the stacking gel was poured on top, and the comb was carefully inserted. Once the stacking gel had polymerized, the gels were stored at 4 °C in a humid atmosphere until use.

The gel cassette was placed into the clamping frame and submerged in 1x electrophoresis buffer prior to electrophoresis. The comb was removed, wells were rinsed with buffer, and 20 µg of protein per sample, prepared during the cell lysis step, was loaded into each well. A prestained protein ladder (Precision Plus Protein™ All Blue, Bio-Rad) was included as a reference. Electrophoresis was run at 20 mA per gel for approximately 2.5 hours, until the dye front reached the bottom of the gel.

5.5.4 Blotting

Separated proteins were transferred from the gel onto a PVDF membrane using a Mini Trans-Blot® Electrophoretic Transfer Cell system. The membrane was first activated by immersing it in methanol for 1 minute, followed by equilibration in blotting buffer. Around 1,000 mL of blotting buffer were prepared, and all subsequent steps were performed submerged to prevent drying or air bubbles and ensure proper equilibration.
The gel was carefully removed from the glass plates and rinsed with water. A “blotting sandwich” was assembled in the gel holder cassette with the black side on the base in the following order: sponge, filter paper, gel, activated membrane, filter paper, and a second sponge. Any air bubbles between the gel and membrane were carefully removed. The closed cassette was then placed into the blotting chamber, which contained an ice block and a magnet stirrer to prevent overheating and ensure uniform buffer circulation. The chamber was filled with blotting buffer, the lid closed, and the assembly connected to the power supply. Proteins were transferred at 100 V for 90 minutes.

5.5.5 Blocking

While the protein transfer was in progress, a 5 % (w/v) milk powder or BSA in 1x TBST was prepared and stirred continuously using a magnetic stir bar on a magnetic stirrer to ensure complete dissolution. After transfer, 25 mL of this solution were transferred into a shallow container, and the PVDF membrane was immersed in the solution. The membrane was incubated for 1 hour at room temperature on a shaker with gentle agitation to block nonspecific binding sites. Following blocking, the membrane was

washed three times for 10 minutes each with 1x TBST to remove unbound blocking solution.

5.5.6 Incubation with primary and secondary antibodies

The PVDF membrane was first incubated with the primary antibody for protein detection. The antibody solution was prepared by dissolving 1 g BSA in 20 mL TBST (5 % w/v), vortexed thoroughly, and 5 mL of this solution were transferred into a 50 mL tube. Then 5 µL of primary antibody were added and mixed by vortexing. The membrane was then immersed in the solution with the protein side facing inward and incubated overnight at 4 °C with gentle rotation. On the following day, the membrane was transferred to a shallow container and washed three times for 10 minutes each with TBST. The secondary antibody solution was prepared similarly by dissolving 1 g milk powder in 20 mL TBST (5 % w/v), vortexed, and 5 mL of this solution were mixed with 5 µL of the appropriate secondary antibody. The membrane was incubated in this solution for 1 hour at room temperature with gentle shaking. Following incubation, the membrane was washed three times for 10 minutes each with TBST.

5.5.7 Detection

A solution for chemiluminescent detection was prepared containing ddH_2O, Tris base (pH 8.5), luminol, and p-coumaric acid.Immediately before application, hydrogen peroxide was added to the solution and briefly mixed. The solution was then applied onto the membrane, which was incubated for 20 seconds, and the chemiluminescent signal was subsequently recorded using Amersham ImageQuant TM 800 (Cytiva, Marlborough, US).

5.5.8 Stripping and probing for the loading control

As a loading control, actin was detected on the membrane. To remove residual primary and secondary antibodies from previous detection, membranes were incubated in 0.5 M NaOH for 10 minutes with gentle shaking, followed by three washes of 10 minutes each with TBST.

For actin detection, the primary antibody was diluted by adding 5 µL of Actin antibody to 5 mL TBST, vortexed briefly, and the membrane was incubated overnight at 4 °C. After incubation, membranes were washed three times for 10 minutes each with TBST. Subsequently, the membrane was incubated with the secondary antibody diluted in milk-TBST for 1 hour at room temperature, followed by three washes with TBST (10 minutes each).

Detection was then performed as described above.

5.6 RNA isolation and RT-qPCR analysis

Technical Equiptment	Provider
LineGene 9600 Plus thermal cycler	BIOER (Hanghzou, China)
C1000TM Thermal Cycler	BIO-RAD Laboratories (Hercules, CA, USA)
DNA/RNA UV-Cleaner box UVT-S-AR	Biosan Medical-Biological Research & Technologies (Riga, Latvia)
HeraeusTM FrescoTM 21 Microcentrifuge	Thermo Fisher Scientific Inc. (Waltham, MA, USA)
HeraeusTM LabofugeTM 400 Centrifuge	Thermo Fisher Scientific Inc. (Waltham, MA, USA)
NanoDropTM 2000c Spectrophotometer	Thermo Fisher Scientific Inc. (Waltham, MA, USA)
qTOWER iris 384	Analytik Jena (Jena, Germany)

Consumables	Provider
White 96- well PCR plates	Biozym Scientific GmbH (Hessisch Oldendorf, Germany)
Transparent adhesive PCR film	Sarstedt AG & Co. KG (Nümbrecht, Germany)
Multiply®-µStrip Pro 8-Strip	Sarstedt AG & Co. KG (Nümbrecht, Germany)
Filter tips (10 µl, 100 µl, 1000 µl)	Sarstedt AG & Co. KG (Nümbrecht, Germany)

Solutions and reagents		Provider
innuPREP RNA Mini Kit 2.0	Lysis Solution RL Washing Solution HS (conc.) Washing Solution LS (conc.) RNase-free Water Spin Filter D	AJ Innuscreen GmbH (Berlin, Germany)

	Spin Filter R Receiver tubes Elution tubes	
High-Capacity cDNA Reverse Transcription Kit	10X RT Buffer 25X dNTP Mix (100 mM) 10X RT Random Primers MultiScribeTM Reverse Transcriptase RNase Inhibitor Nuclease-free H2O	Thermo Fisher Scientific Inc. (Waltham, MA, USA)
2X Luna® Universal qPCR Master Mix		New England Biolabs (Ipswich, MA, USA)

Primers Target/sequence	**Provider**
β-Actin fw: CACCATTGGCAATGAGCGGTTC rv: AGGTCTTTGCGGATGTCCACGT	Invitrogen, via Thermo Fisher Scientific Inc. (Waltham, MA, USA)
CYP1A1 fw: GATTGAGCACTGTCAGGAGAACG rv: ATGAGGCTCCAGGAGATAGCAG	Invitrogen, via Thermo Fisher Scientific Inc. (Waltham, MA, USA)
ZO1 fw: GTCCAGAATCTCGGAAAAGTGCC rv: CTTTCAGCGCACCATACCAACC	Invitrogen, via Thermo Fisher Scientific Inc. (Waltham, MA, USA)
TI-PARP Fw: GATTCTCAGGAGCACTTGGAAAG Rv : TGGTTGGACAGCCTTCTAGT	Invitrogen, via Thermo Fisher Scientific Inc. (Waltham, MA, USA)

5.6.1 RNA Isolation

Total RNA from treated cells was isolated using the innuPREP RNA Mini Kit 2.0 (AJ Innuscreen GmbH) according to the manufacturer's instructions. To minimize the risk of contamination, only RNase-free consumables and filtered pipette tips were used throughout the procedure.

Cell pellets were lysed by adding 400 µL of Lysis Solution RL and incubating the samples for 2 minutes. The pellets were then completely resuspended by repeated pipetting and incubated for an additional 3 minutes. The lysates were transferred to Spin Filter D columns placed in receiver tubes and centrifuged at 11.000 x g for 2 minutes. After centrifugation, the Spin Filter D columns were discarded.

400 µL of 70 % ethanol were added and mixed thoroughly by pipetting. The mixture was subsequently loaded onto Spin Filter R columns placed in receiver tubes and centrifuged at 11.000 x g for 2 minutes. The flow-through was discarded, and the columns were washed with 500 µL of high-stringency washing solution (HS) followed by centrifugation at 11.000 x g for 1 minute. After discarding the filtrate, a second wash was performed using 700 µL of low-stringency washing solution (LS) and centrifugation at 11.000 x g for 1 minute. This washing step was repeated once using 700 µL of 80 % ethanol.

To remove residual ethanol, the columns were centrifuged at 11.000 x g for 3 minutes. The receiver tubes containing the filtrate were discarded, and the Spin Filter R columns were transferred to clean elution tubes. RNA was eluted by adding 30 µL of nuclease-free water, incubating for 1 minute at room temperature, and centrifuging at 11.000 x g for 1 minute. The purified RNA was collected in the elution tubes.

The concentration of the purified RNA was determined spectrophotometrically using a NanoDrop 2000c. Measurements were performed at 260 nm, and RNA concentration was calculated based on the absorbance at 260 nm (A260). Purity was assessed by determining the A260/A280 and A260/A230 ratios. For double-stranded DNA, an absorbance of 1.0 at 260 nm corresponds to a concentration of 50 µg/mL, for RNA it corresponds to 40 µg/mL-
Following quantification, the isolated RNA was stored at −80 °C.

5.6.2 cDNA synthesis

Complementary DNA (cDNA) was generated from the isolated RNA by reverse transcription. Prior to the reaction, the required volumes of RNA sample and nuclease-

free water were calculated to obtain 1 µg of RNA in a total volume of 10 µL per sample. All preparation steps were carried out in a DNA/RNA UV-clean bench to avoid contamination. Throughout the procedure, samples and reagents were maintained on ice or in a PCR chiller. A reverse transcription master mix was prepared as described below.

Component	Volume
10x RT Buffer	2 µl
25x dNTP Mix	0,8 µl
10x RT Primers	2 µl
RT	1 µl
Nuclease-free H2O	4,2 µl
RNA	1 µg in 10 µl
Total	**20 µL**

The components of the reverse transcription reaction were combined to prepare a master mix, and 10 µL of the mixture were dispensed into each PCR tube. The previously calculated volume of RNA corresponding to 1 µg per sample was then added and filled up with nuclease-free water up to a final volume of 20 µL.

The reactions were gently mixed by repeated pipetting and briefly centrifuged at 1,000 x g for 1 minute. cDNA synthesis was subsequently carried out using a C1000™ Thermal Cycler under the conditions described below.

Step 1	**Step 2**	**Step 3**	**Step 4**
25.0° C	37° C	85° C	4° C
10 min	120 min	5 min	forever

Following the addition of 30 µL of nuclease-free water, resulting in a final volume of 50 µL (20 ng/µL RNA), the samples were stored at −80 °C until further use.

5.6.3 RT-qPCR

Quantitative polymerase chain reaction (qPCR) was performed with the previously synthesized cDNA to amplify and quantify specific gene expression using specific primers and a DNA-binding fluorescent dye. During amplification, the increase in fluorescence intensity correlates with the amount of amplified DNA, allowing quantitative analysis of gene expression.

All experimental steps were carried out in a DNA/RNA-clean workbench to prevent contamination, and samples as well as reagents were maintained on ice or in a PCR chiller throughout the procedure. For each target gene, a separate master mix was prepared as described below.

Component	Volume
2x Luna Master Mix	7.5 µL
10 µM Primer fv	0.75 µL
10 µM Primer rv	0.75 µL
Nuclease-free H2O	4.0 µL
cDNA	2 µL

Each reaction contained 13 µL of the prepared master mix and 2 µL of cDNA, dispensed into wells of a 96-well PCR plate in technical triplicates. The plate was sealed with adhesive PCR film, briefly centrifuged at 1,000 x g for 1 minute, and placed into the qPCR instrument.

The amplification protocol consisted of an initial denaturation step at 95 °C for 1 minute, followed by 45 cycles of denaturation at 95 °C for 15 seconds and annealing at 60 °C for 30 seconds. Upon completion of amplification, a melting curve analysis was performed with incubation at 95 °C for 15 seconds and 55 °C for 30 seconds.

5.6.4 Data Analysis

Each experimental condition was analyzed in three technical replicates. During amplification, fluorescence signals were recorded at every cycle, and relative mRNA expression levels were determined using the $2^{-\Delta\Delta Ct}$ approach. Target gene Ct values were first normalized to the housekeeping gene Actin and then compared to the corresponding control group. Because the ΔΔCt value of the calibrator sample is zero, its relative expression was set to 1.0 for presentation purposes. Accordingly, fold changes in gene expression were calculated using the $2^{-\Delta\Delta Ct}$ formula.

Statistical evaluation and data visualization were performed using GraphPad Prism 9.

6 References

(1) Zinecker, H.; Simon, A. K. Autophagy Takes It All – Autophagy Inducers Target Immune Aging. Dis. Model. Mech. 2022, 15, dmm049345. https://doi.org/10.1242/dmm.049345

(2) Dominguez, L. J.; Veronese, N.; Baiamonte, E.; Guarrera, M.; Parisi, A.; Ruffolo, C.; Tagliaferri, F.; Barbagallo, M. Healthy Aging and Dietary Patterns. Nutrients 2022, 14, 4026. https://doi.org/10.3390/nu14194026

(3) Behr, L. C.; Simm, A.; Kluttig, A.; Grosskopf, A. 60 Years of Healthy Aging: On Definitions, Biomarkers, Scores and Challenges. Aging (Albany NY) 2022, 14 (16), 6461–6483. https://doi.org/10.18632/aging.204248

(4) Menassa, M.; Stronks, K.; Khatmi, F.; Roa Díaz, Z. M.; Pano Espinola, O.; Gamba, M.; Itodo, O. A.; Butti, C.; Wehrli, F.; Minder, B.; Rivas Velarde, M.; Franco, O. H. *Concepts and Definitions of Healthy Ageing: A Systematic Review and Synthesis of Theoretical Models*. eClinicalMedicine 2023, 56, 101821. https://doi.org/10.1016/j.eclinm.2022.101821

(5) Schmauck-Medina, T.; Molière, A.; Lautrup, S.; Zhang, J.; Chlopicki, S.; Madsen, H. B.; Cao, S.; Soendenbroe, C.; Mansell, E.; Vestergaard, M. B.; Li, Z.; Shiloh, Y.; Opresko, P. L.; Egly, J.-M.; Kirkwood, T.; Verdin, E.; Bohr, V. A.; Cox, L. S.; Stevnsner, T.; Rasmussen, L. J.; Fang, E. F. *New Hallmarks of Ageing: A 2022 Copenhagen Ageing Meeting Summary*.

(6) Kaushik, S.; Tasset, I.; Arias, E.; Pampliega, O.; Wong, E.; Martinez-Vicente, M.; Cuervo, A. M. *Autophagy and the Hallmarks of Aging*. Ageing Res. Rev. 2021, 72, 101468. https://doi.org/10.1016/j.arr.2021.101468

(7) Aman, Y.; Schmauck-Medina, T.; Hansen, M.; Morimoto, R. I.; Simon, A. K.; Bjedov, I.; Palikaras, K.; Simonsen, A.; Johansen, T.; Tavernarakis, N.; Rubinsztein, D. C.; Partridge, L.; Kroemer, G.; Labbadia, J.; Fang, E. F. *Autophagy in Healthy Aging and Disease*. Ageing Res. Rev. 2021, 72, 101468. https://doi.org/10.1016/j.arr.2021.101468

(8) He, C. *Autophagy: Nutrient and Energy Mobilization in Need*. Curr. Biol. 2022, 32 (12), R684–R696. https://doi.org/10.1016/j.cub.2022.04.071.

(9) Raben, N.; Puertollano, R. *TFEB and TFE3: Linking Lysosomes to Cellular Adaptation to Stress*. Annu. Rev. Cell Dev. Biol. 2016. https://doi.org/10.1146/annurev-cellbio-111315-125407.

(10) Chen, H.; Gong, S.; Zhang, H.; Chen, Y.; Liu, Y.; Hao, J.; Li, X.; Liu, H. *From the Regulatory Mechanism of TFEB to Its Therapeutic Implications*. © The Author(s) 2024.

(11) Chen, M.; Dai, Y.; Liu, S.; Fan, Y.; Ding, Z.; Li, D. *TFEB Biology and Agonists at a Glance*. Cells 2021, 10 (2). https://doi.org/10.3390/cells10020333.

(12) Abudahab, S.; Price, E.T.; Dozmorov, M.G.; Deshpande, L.S.; McClay, J.L. The Aryl Hydrocarbon Receptor, Epigenetics and the Aging Process. *J Nutr Health Aging* 2023, 27(4), 291–300. https://doi.org/10.1007/s12603-023-1908-1

(13) Zimniak, P. Detoxification reactions: relevance to aging. *Ageing Res Rev* 2008, 7(4), 281–300. https://doi.org/10.1016/j.arr.2008.04.001

(14) López-Otín C. et al. (2013). *The Hallmarks of Aging*. Cell. doi:10.1016/j.cell.2013.05.039

(15) Gladyshev V.N. (2016). *Aging: progressive decline in fitness due to molecular damage*. Aging Cell. doi:10.1111/acel.12480

(16) Zimniak P. (2008). *Detoxification reactions: relevance to aging*. Ageing Research Reviews. doi:10.1016/j.arr.2008.04.001

(17) Schmucker D.L., Sanchez H. (2011). *Liver regeneration and aging: implications for detoxification capacity*. Exp Gerontol. doi:10.1016/j.exger.2011.02.006

(18) Misra JR, Horner MA, Lam G, Thummel CS. (2011). Transcriptional regulation of xenobiotic detoxification in Drosophila. *Genes & Development*. 25(17): 1796–1806. doi:10.1101/gad.17206011

(19) Fukushige T, Smith HE, Miwa J, Krause MW, Hanover JA. (2017). A genetic analysis of the *Caenorhabditis elegans* detoxification response. *Genetics*. 206(2): 939–955. doi:10.1534/genetics.117.202515

(20) Crocco P, Montesanto A, Dato S, Geracitano S, Iannone F, Passarino G, Rose G. (2019). Inter-individual variability in xenobiotic-metabolizing enzymes: implications for human aging and longevity. *International Journal of Molecular Sciences*. 20(15): 3709. doi:10.3390/ijms20153709

(21) Hoffmann JM, Partridge L. (2015). Nuclear hormone receptors: roles of xenobiotic detoxification and sterol homeostasis in healthy aging. *Critical Reviews in Biochemistry and Molecular Biology*. 50(5): 380–392. doi:10.3109/10409238.2015.1067186

(22) Serna E, Cespedes C, Vina J. (2021). Anti-aging physiological roles of aryl hydrocarbon receptor and its dietary regulators. *International Journal of Molecular Sciences*. 22(1): 374. doi:10.3390/ijms22010374

(23) Huchzermeier R, van der Vorst EPC. Aryl hydrocarbon receptor (AHR) and nuclear factor erythroid-derived 2-like 2 (NRF2): An important crosstalk in the gut-liver axis. Biochemical Pharmacology. 2025;116785. doi:10.1016/j.bcp.2025.116785

(24) Degrelle SA, Ferecatu I, Fournier T. Novel fluorescent and secreted transcriptional reporters for quantifying activity of the xenobiotic sensor aryl hydrocarbon receptor (AHR). Environment International. 2022;107545. doi:10.1016/j.envint.2022.107545

(25) Rakateli L, Huchzermeier R, van der Vorst EPC. AhR, PXR and CAR: From xenobiotic receptors to metabolic sensors. Cells. 2023;12(23):2752. doi:10.3390/cells12232752

(26) Avilla MN, Malecki KMC, Hahn ME, Wilson RH, Bradfield CA. The Ah receptor: Adaptive metabolism, ligand diversity, and the xenokine model. Chemical Research in Toxicology. 2020;33(4):860–879. doi:10.1021/acs.chemrestox.9b00476

(27) Pinto CJG, Avila-Gálvez MÁ, Nunes dos Santos C. Targeting the aryl hydrocarbon receptor by gut phenolic metabolites: A strategy towards gut inflammation. Redox Biology. 2023;102622. doi:10.1016/j.redox.2023.102622

(28) Rothhammer V, Quintana FJ. The aryl hydrocarbon receptor: an environmental sensor integrating immune responses in health and disease. Nature Reviews Immunology. 2019;19(3):184–197. doi:10.1038/s41577-019-0125-8

(29) Shimada T, Fujii-Kuriyama Y. Metabolic activation of polycyclic aromatic hydrocarbons to carcinogens by cytochromes P450 1A1 and 1B1. Cancer

Science. 2004;95(1):1–6.
https://doi.org/10.1111/j.1349-7006.2004.tb03162.x

(30) Bjeldanes LF, et al. Indole-3-carbinol and its condensation products: implications for cancer prevention and therapy. Journal of Nutrition. 2001;131(11):2985S–2991S.
https://doi.org/10.1093/jn/131.11.2985S

(31) Rannug A, Rannug U, Rosenkranz HS, et al. Certain photoproducts of tryptophan bind with very high affinity to the Ah receptor and are likely to be endogenous signal substances. Journal of Biological Chemistry. 1987;262(32):15422–15427.
https://www.jbc.org/content/262/32/15422

(32) Nguyen LP, Bradfield CA. The search for endogenous activators of the aryl hydrocarbon receptor. Chemical Research in Toxicology. 2008;21(1):102–116.
https://doi.org/10.1021/tx7001965

(33) Wincent E, et al. Inhibition of cytochrome P4501-dependent clearance of the endogenous Ah receptor agonist FICZ as a mechanism for activation of the Ah receptor. Proceedings of the National Academy of Sciences USA. 2009;106(21):1–6.
https://doi.org/10.1073/pnas.0901652106

(34) Zoncu R, Bar-Peled L, Efeyan A, Wang S, Sancak Y, Sabatini DM. Amino acid sensing in mTORC1 signaling. *Cell*. 2011;146(5): 722–733.
https://doi.org/10.1016/j.cell.2011.06.035

(35) Findlay GM, Yan L, Procter J, Mieulet V, Lamb RF. A MAP4 kinase related to Ste20 is a nutrient-sensitive regulator of mTOR signalling. *Biochemical Journal*. 2007;403(1): 13–20. https://doi.org/10.1042/BJ20061874

(36) Napolitano G, Di Malta C, Esposito A, et al. mTOR-dependent phosphorylation controls TFEB nuclear export. *EMBO Journal*. 2018;37(11): e99062. https://doi.org/10.15252/embj.201899062

(37) Medina DL, Di Paola S, Peluso I, et al. Lysosomal calcium signalling regulates autophagy through calcineurin and TFEB. *Nature Cell Biology*. 2015;17(3): 288–299. https://doi.org/10.1038/ncb3114

(38) Palmieri M, Pal R, Nelvagal HR, et al. TFEB biology and agonists at a glance. *Cells*. 2021;10(2): 333. https://doi.org/10.3390/cells10020333

(39) Settembre C, Di Malta C, Polito VA, et al. TFEB controls cellular clearance by promoting the expression of autophagy and lysosomal biogenesis genes. *Science*. 2011;332(6036):1429–1433. https://doi.org/10.1126/science.1204592

(40) Martina JA, Chen Y, Gucek M, Puertollano R. MTORC1 functions as a transcriptional regulator of autophagy by preventing nuclear transport of TFEB. *Autophagy*. 2012;8(6):903–914. https://doi.org/10.4161/auto.19653

(41) Medina DL, Di Paola S, Peluso I, et al. Lysosomal calcium signalling regulates autophagy through calcineurin and TFEB. *Nature Cell Biology*. 2015;17(3):288–299. https://doi.org/10.1038/ncb3114

(42) Song J-X, Sun Y-R, Peluso I, et al. A novel curcumin analog binds to and activates TFEB in vitro and in vivo independent of MTOR inhibition. Autophagy. 2016;12(8):1372–1389. https://doi.org/10.1080/15548627.2016.1179404

(43) Rehman A, Koh Y-S. Aryl Hydrocarbon Receptor, a Critical Interface between Host Immunity and Microbiota. Journal of Bacteriology and Virology. 2025;55(4):298–308. https://doi.org/10.4167/jbv.2025.55.4.298

(44) Chen I, Safe S, Bjeldanes LF. *Indole-3-carbinol and diindolylmethane as aryl hydrocarbon (Ah) receptor agonists and antagonists in T47D human breast cancer cells*. Biochemical Pharmacology. 1996;51(8):1069-1076. https://doi.org/10.1016/0006-2952(96)00060-3

(45) Vega-Rubin-de-Celis S, Peña-Llopis S, Konda M, Brugarolas J. Multistep regulation of TFEB by mTORC1. Autophagy. 2017;13(3):464–472. https://doi.org/10.1080/15548627.2016.1271514

(46) Luo, L., & Qin, Z.-H. (2019). *Autophagy, Aging, and Longevity*. Advances in Experimental Medicine and Biology, 1206, 509–525. https://doi.org/10.1007/978-981-15-0602-4_24

(47) Harrison, D. E.; Strong, R.; Sharp, Z. D.; Nelson, J. F.; Astle, C. M.; Flurkey, K.; Nadon, N. L.; Wilkinson, J. E.; Frenkel, K.; Carter, C. S.; Pahor, M.; Javors, M. A.; Fernandez, E.; Miller, R. A. Rapamycin Fed Late in Life Extends Lifespan in

Genetically Heterogeneous Mice. *Nature* 2009, 460 (7253), 392–395. https://doi.org/10.1038/nature08221

(48) Peterson, T. R., Laplante, M., Thoreen, C. C., Sancak, Y., Kang, S. A., Kuehl, W. M., Gray, N. S., & Sabatini, D. M. (2009). DEPTOR is an mTOR inhibitor frequently overexpressed in multiple myeloma cells and required for their survival. *Journal of Biological Chemistry, 284*(9), 8022–8032. https://doi.org/10.1074/jbc.M900388200

(49) Thoreen, C. C., Kang, S. A., Chang, J. W., Liu, Q., Zhang, J., Gao, Y., Reichling, L. J., Sim, T., Sabatini, D. M., & Gray, N. S. (2009). An ATP-competitive mammalian target of rapamycin inhibitor reveals rapamycin-resistant functions of mTORC1. *Cell, 137*(6), 873–886. https://doi.org/10.1016/j.cell.2009.03.014

(50) Feldman, M. E., Apsel, B., Uotila, A., Loewith, R., Knight, Z. A., Ruggero, D., & Shokat, K. M. (2009). Active-site inhibitors of mTOR target rapamycin-resistant outputs of mTORC1 and mTORC2. *PLoS Biology, 7*(2), e1000039. https://doi.org/10.1371/journal.pbio.1000039

(51) Martina, J. A., Chen, Y., Gucek, M., & Puertollano, R. (2012). MTORC1 functions as a transcriptional regulator of autophagy by controlling TFEB. *Nature Cell Biology, 14*(12), 123–133. https://doi.org/10.1038/ncb2551

(52) Settembre, C., Di Malta, C., Polito, V. A., Garcia Arencibia, M., Vetrini, F., Erdin, S., … & Ballabio, A. (2012). TFEB links autophagy to lysosomal biogenesis. *Science, 332*(6036), 1429–1433. https://doi.org/10.1126/science.1204592

(53) Satsu, H., Yoshida, K., Mikubo, A., et al. Establishment of a stable aryl hydrocarbon receptor-responsive HepG2 cell line. *Cytotechnology*, 67(4), 621–632 (2015). https://doi.org/10.1007/s10616-014-9711-6

(54) Tian, Y., Gui, W., Smith, P. B., Koo, I., Murray, I. A., Cantorna, M. T., Perdew, G. H., & Patterson, A. D**.** Isolation and Identification of Aryl Hydrocarbon Receptor Modulators in White Button Mushrooms (*Agaricus bisporus*). *Journal of Agricultural and Food Chemistry*, 67(33), 9286–9294 (2019). https://doi.org/10.1021/acs.jafc.9b03212

(55) Pinto, J.P., et al. *Targeting the aryl hydrocarbon receptor by gut phenolic metabolites: A strategy towards gut inflammation*. Redox Biology, 2023. https://doi.org/10.1016/j.redox.2023.102622

(56) Auld, D. S., & Inglese, J. Interferences with Luciferase Reporter Enzymes. In: Markossian, S., Grossman, A., Baskir, H., et al. (Eds.), *Assay Guidance Manual*. Bethesda (MD): Eli Lilly & Company and the National Center for Advancing Translational Sciences (2016). https://www.ncbi.nlm.nih.gov/books/NBK374281/

(57) Laplante, M., Sabatini, D.M. mTOR signaling in growth control and disease. *Cell*, 2012. https://doi.org/10.1016/j.cell.2012.03.019

(58) Thoreen, C.C., et al. An ATP-competitive mTOR inhibitor reveals rapamycin-resistant functions of mTORC1. *Nature*, 2009. https://doi.org/10.1038/nature07565

7 List of Figures